nature communications

Article

https://doi.org/10.1038/s41467-026-68937-9

Gut microbiota-dependent 24-hydroxycholesterol metabolism contributes to capsaicin-induced amelioration of Alzheimer's disease-like pathology in mice

Received: 6 March 2025

Accepted: 21 January 2026

Published online: 03 February 2026

Check for updates

Yawen Li[1,2,17], Hui Wang[3,4,5,6,17], Dongyuan Zhang[3,4,5,6,17], Shiqi Wang[3,4,5,17], Zheng Li[7,8,9], Jingjie Li[7,8,9], Shentao Tai[1], Dandan Tong[1], Bifeng Wang[1], Dingbing Lu[1], Shulu Yuan[3,4,5], Weiqi Sun[3,4,5], Biyu Yang[3,4,5], Chaobo Bai[10], Qi Wang[10], Jiuyang Ding[11,12], Zhihao Wang[13,14], Yang Gao[15], Haitao Yu[16], Kun Cui[6], Chang Liu[6], Jian Mao[6], Yun Yao[3,4,5], Fengyu Liu[3,4,5], You Wan[3,4,5,6], Junliang Yuan[10] ✉, Xuemei Liu[1,2] ✉ & Jie Zheng[3,4,5,6] ✉

Dietary capsaicin intake appears to affect the pathogenesis of Alzheimer's disease (AD), while the underlying mechanisms remain unclear. Here, we found in human cohorts that moderate-to-high level of dietary capsaicin intake was associated with improved cognitive performance. Similarly, long-term oral capsaicin administration in male 5×FAD mice ameliorated AD-like pathologies and reshaped gut microbial composition. Gut microbiota transfer from capsaicin-treated mice produced similar effects of capsaicin intake. Moreover, capsaicin elevated the level of host 24(S)-hydroxycholesterol (24-HC), relating to the increase of gut *Oscillibacter* genus abundance. The 24-HC elevation enhanced microglial phagocytic activity in the brain, and inhibited proinflammatory factors production via liver x receptor β (LXRβ)-mediated transcriptional regulation. Finally, we observed elevation of 24-HC in plasma in AD patients with higher level of dietary capsaicin intake, which correlated with cognitive scores and plasma Aβ and p-tau biomarkers. These findings suggest the potential of capsaicin or capsaicin-rich diets in the prevention or treatment of AD and related diseases.

Alzheimer's disease (AD) is the most common cause of dementia in the elderly, with extracellular deposition of beta-amyloid (Aβ) and intraneuronal accumulation of hyperphosphorylated tau protein in the brain as two pathologic hallmarks[1]. There is no cure for AD to date[2]. In recent years, increasing attention has been paid to the influences of dietary pattern on AD onset and development[3,4]. Especially, emerging evidences have suggested a significant correlation of AD pathogenesis with dietary intake of capsaicin from chili peppers-rich foods[5], which are prevalent in a number of regions worldwide including the Southwest China. Natural and synthetic capsaicin analogs showed many protective effects like antioxidation and anti-inflammation that potentially reduce the risk or degree of AD[6]. However, the exact protective effect and underlying mechanisms of capsaicin against AD are still elusive.

It has been recently unveiled that gut bacterial profile had strongly links to the development of AD[7]. Gut dysbiosis like imbalance between the *Firmicutes* and *Bacteroidetes* was widely recognized both in AD patients and animal models, which was even observed at the

A full list of affiliations appears at the end of the paper. ✉e-mail: junliangyuan@bjmu.edu.cn; onlyoneliuxuemei@163.com; zhengjiie@hsc.pku.edu.cn

preclinical stage[8,9]. Transplantation of fecal microbiota from AD patients or transgenic mice both induced AD-like pathologies in microbiota-depleted healthy mice[10–13], conversely, fecal microbiota transfer from wild-type mice and direct gavage of probiotics like *Lactobacillus* and *Bifidobacterium* both produced anti-AD outcomes[14,15]. Of note, capsaicin intake through diets appeared to be capable of reshaping the constitution and function of gut microbes[16], but whether and how it contributes to the potential anti-AD effect of capsaicin are unknown.

The contribution of gut microbiota malfunction to AD pathogenesis is mainly mediated by the dysregulation of host metabolism. For example, gut dysbiosis in AD mice elevated levels of 12-hydroxyheptadecatrienoic acid, prostaglandin E2 and poly-unsaturated fatty acids to elicit microglia overactivation and exacerbate AD symptoms in the brain[10,12]. Moreover, some gut microbes were capable of directly metabolizing diet-derived cholesterol through bacterial enzymes[17–20], which might thereby regulate pathological processes like Aβ deposition, tau hyperphosphorylation and neuroinflammation[21,22]. Nonetheless, it is unknown how oral intake of capsaicin modulates host metabolism in a gut microbiota-dependent way to affect the AD pathogenesis.

In this work, we seek to investigate the effect and mechanism of oral capsaicin intake in affecting AD pathogenesis, and found in human cohorts that moderate-to-high dietary capsaicin consumption was associated with improved cognitive performance. Similarly, long-term oral capsaicin administration in 5×FAD mice alleviated AD-like pathologies. Unexpectedly, these protective effects of capsaicin persisted following global knock-out of capsaicin receptor TRPV1. Further studies revealed that the gut microbiota, especially the *Oscillibacter* genus had an important contribution to the protective effects of capsaicin, which modulated lipid metabolism to elevate host 24(S)-hydroxycholesterol (24-HC) level, thereby enhancing microglial phagocytic activity in the brain, and facilitating the liver x receptor β (LXRβ)-mediated transcriptional inhibition of proinflammatory factors production. These findings suggest a way of capsaicin to alleviate AD pathologies through gut microbiome-dependent regulation on 24-HC metabolism, and the potential of capsaicin or capsaicin-rich diets in the prevention or treatment of AD and related diseases.

Results

Capsaicin intake correlates with cognitive improvements in AD patients and 5×FAD mice

Firstly, we accessed the association between the dietary capsaicin intake levels and cognitive function in two Chinese cohorts ($N = 151$ and 95, respectively). Subject information of sex, age, education level etc. was summarized in the Supplementary Data 1. Cognitive function was assessed using Mini-Mental State Examination (MMSE) and / or Montreal Cognitive Assessment (MoCA). The cohorts consisted of subjects diagnosed to be cognitively normal (CN), with mild cognitive impairments (MCI), moderate to severe cognitive impairment (M/SCI) based on MMSE scores, or definite AD based on comprehensive clinical assessment. Capsaicin intake in diets were evaluated using a self-developed scale (Supplementary Data 2). The results showed that subjects with moderate-to-high levels of chili intake had higher cognitive scores in subgroups with cognitive impairments and AD patients following adjustment of other covariates including sex, age, education years, hypertension, diabetes, coronary heart disease and gastritis in the analysis of covariance (ANCOVA) (Fig. 1a, Supplementary Data 3). In addition, we also evaluated the preference and tolerance to chili-rich diets, which were both found to tightly correlate with the intake level of chili-rich diets, and slightly correlate with cognitive scores, respectively. Besides, there was lower prevalence of AD in the subgroup with moderate-to-high level of chili intake (Supplementary Fig. S1).

Next, we examined the potential dose-dependent effect of dietary capsaicin (abbreviated as Cap in figures) intake in 3-month-old wild-type (WT) C57BL/6 mice, increasing doses of capsaicin (0.01 – 1 mg/kg) were administrated intragastrically (i.g.) once every day for a month. We found that capsaicin at 1 mg/kg, but not at lower doses, had the tendency to facilitate object-place recognition, novel-object recognition of mice, and to enhance spatial memory in Morris-water maze test. By contrast, capsaicin at all doses did not affect contextual fear memory. Additionally, capsaicin also increased the time of mice spent in the central zone in open field test, and time in the open arms in elevated-plus maze test, possibly thanks to the decrease in anxiety following capsaicin (Supplementary Fig. S2).

In subsequent, we treated 5-month-old WT and 5×FAD mice, a transgenic line expressing human APP and PSEN1 with a total of five AD-linked mutations[23], with capsaicin at the dosage of 1 mg/kg for a month (Fig. 1b). Capsaicin again showed trends in improving object-place recognition and spatial memory Morris-water maze in WT mice, and more importantly, it alleviated cognitive impairments of 5xFAD mice in these behavioral tests (Fig. 1c–i). Moreover, capsaicin also increased the discriminative index in the novel-object recognition test, but did not change conditioned contextual fear memory (Supplementary Fig. S3a-b). Intriguingly, by contrast to WT mice, capsaicin had only limited effects on the anxiety-like behaviors of 5×FAD mice in both open-field and elevated-plus maze tests (Supplementary Fig. S3c-d), which might be attributed to the hyperactivity of this transgenic line at early age[24].

Capsaicin reduces Aβ burden and inhibits microglia over-activation in the hippocampus of 5xFAD mice

In consistent with the capsaicin-induced improvements in cognitive functions of 5×FAD mice, we found that capsaicin decreased the density of beta-amyloid (Aβ) plaques stained by 6E10 antibody in the hippocampus of brain, and downregulated both the levels of SDS-insoluble and soluble Aβ40 and Aβ42 fragments (Fig. 1j–l, supplementary Fig. S3e). Of note, capsaicin did not change total protein levels of Aβ precursor protein (APP), β-Site APP cleaving enzyme 1 (BACE1) and presenilin-1 (PSEN1) (Supplementary Fig. S3f-g), suggesting non-significant change in the production of Aβ.

Subsequently, we analyzed the capsaicin-induced transcriptomic changes in the hippocampus of 5×FAD mice by bulk RNA sequencing, and found that differentially expressed genes (DEGs) were predominantly enriched in GO_biological pathways involved in immune and inflammatory regulation (Supplementary Fig. S3h), and the majority of these DEGs were downregulated in the Cap-treated group (Supplementary Data 4). We measured local levels of pro-inflammatory factors interleukin 1β (IL-1β) and tumor necrosis factor alpha (TNF-α) in the hippocampus of 5×FAD mice utilizing enzyme-linked immunosorbent assay (ELISA), and found these two factors were both downregulated by capsaicin (Supplementary Fig. S3i), suggesting an anti-inflammatory effect of capsaicin in the brain.

It has been well-recognized in AD brains that overactivation of microglia, the major type of immune cell in central nervous system, impairs its capacity of Aβ phagocytosis and amplifies neuroinflammatory responses[25]. Thereby, we examined how capsaicin affected microglia. On one hand, capsaicin decreased the number of plaque-surrounded cell aggregates of microglia, which was consistent with the reduction of plaque numbers (Fig. 1m, n). On the other hand, for separated microglia that were not clustered around plaques, capsaicin intake decreased the volume of soma but increased the branching complexity of cell processes (Fig. 1o, p), these morphologic signs all suggested suppression of microglia overactivation[26].

To examine whether the capsaicin-induced suppression of microglia activation and inflammation in 5×FAD mice was a primary outcome or merely a secondary consequence following Aβ plaques reduction, we administrated capsaicin in 3-month-old WT C57BL/6 mice with repeat intraperitoneal (i.p.) injections of lipopolysaccharide (LPS), a model showing central neuroinflammation but no Aβ

deposition[27]. We found in these mice that capsaicin treatment still showed effectiveness in downregulation IL-1β and TNF-α, and in decreasing microglia activation in the hippocampus (Supplementary Fig. S4). These results suggest that the observed anti-inflammatory effects of capsaicin in 5×FAD mice occurred at least partly in prior to the reduction of Aβ plaques.

Knock-out of TRPV1 has limited impact on the protective effects of capsaicin against AD

To investigate mechanisms underlying the protective effects of capsaicin in AD mice, we firstly measured the distribution of capsaicin in 5×FAD mice following repeated oral administration. The results showed that capsaicin was enriched in the contents of stomach and gut, and to relatively less concentration contained in tissues of stomach, intestines, liver and brain (Fig. 2a).

To examine whether the anti-AD effects of capsaicin was dependent on its binding to the well-recognized capsaicin receptor, transient receptor potential vanilloid sub-type1 (TRPV1), especially in the stomach and intestines, we generated a mouse line of 5×FAD mice with global TRPV1 gene knock-out, termed 5×FAD & TRPV1$^{-/-}$ (5×FAD & KO) (Fig. 2b–d). Unexpectedly, we found both in Veh- and Cap-treated 5XFAD mice at 6-month of age that TRPV1 KO changed none of Aβ

Fig. 1 | Capsaicin intake improves cognitive function in AD patients and ameliorates brain pathologies in 5×FAD mice. a Human subjects with moderate-to-high dietary chili intake had higher MMSE and MoCA scores in MCI or AD subsets. Data are presented as median with quartiles. $n = 145$ (cohort 1) or 95 (cohort 2) in total. ANCOVA with sex, age, education years, hypertension, diabetes, coronary heart disease, and gastritis as covariates, followed by two-sided Bonferroni-corrected multiple comparisons to evaluate treatment differences within each of the three major groups. CN, cognitively normal. MCI, mild cognitive impairment. AD, Alzheimer's disease. **b** Experimental schedule of capsaicin (Cap) or vehicle (Veh) administration in wild-type (WT) and 5×FAD mice. **c**–**e** Capsaicin increased bias score of WT and 5×FAD mice in the object-place recognition test. The cartoon (**c**) shows the paradigm of behavioral test. Representative heatmaps (**d**) show time distribution of mice spent in the chamber during the test phase. Data are presented as mean ± SD. $n = 8$ mice in each group. Two-way ANOVA followed by Tukey's multiple comparisons tests. **f** A cartoon showing the experimental paradigm of Morris water maze test. **g** Capsaicin increased the efficiency of 5×FAD mice learning to find the hidden platform during training phase in Morris water maze test. $n = 8$ mice in each group. Data are presented as mean ± SD. two-way ANOVA followed by Tukey's multiple comparisons tests. WT+Veh *vs* WT+Cap, n.s. $P = 0.917$; WT+Veh vs 5×FAD+Veh, $^{**}P = 0.0002$; 5×FAD +Veh *vs* 5×FAD+Cap, $^{**}P = 0.001$. **h**, **i** Capsaicin increased the time of both WT and 5×FAD mice spent in the target quadrate during the test phase of Morris water maze test. Representative trajectory maps show trace of mice traveled in the maze, and cyan areas indicate the target quadrant in water maze (i). $n = 8$ mice in each group. Data are presented as mean ± SD. Two-way ANOVA followed by Tukey's multiple comparisons tests. **j**–**k** Capsaicin decreased the amount of Aβ plaques in 5xFAD mice. Representative images (**j**) show 6E10-stained plaques. Black boxes indicate the areas zoomed in on right. $n = 4$ mice in each group. Data are presented as mean ± SD. Two-way ANOVA followed by Tukey's multiple comparisons tests. **l** Capsaicin decreased the levels of sodium dodecyl sulfate (SDS)-insoluble $A\beta_{40}$ and $A\beta_{42}$ in 5xFAD mice. $n = 4$ mice in each group. Data are presented as mean ± SD. Two-way ANOVA followed by Tukey's multiple comparisons tests. **m** Representative images of Iba1 immunofluorescent staining and 3D morphological reconstruction of microglia. White circles indicate plaque-surrounded cell aggregates, arrows point to representative cells showed in reconstructed images. Capsaicin did not change microglia morphology in WT mice, but decreased number of plaque-surrounded microglia aggregates (**n**), decreased soma volume (**o**) and increase cell process branching complexity (**p**) of separated microglia in 5xFAD mice. Gray crosses indicate individual cells and circles indicate mean values of individual mouse (**o**). Bands indicate SD (**p**). $n = 4$ mice or 20 cells per group. Data are presented as mean ± SD. Two-way ANOVA followed by Tukey's multiple comparisons tests. For statistics in panel (**p**), WT+Veh vs WT+Cap, $P = 0.824$ (n.s.); WT+Veh vs 5×FAD+Veh, $^{**}P = 0.0001$; 5×FAD +Veh vs 5×FAD+Cap, $^{**}P = 0.0001$. Source data are provided as a Source Data file. Certain illustrative components in panels (**b**, **c**, and **f**) are created in BioRender. Zheng, J. (2026) https://BioRender.com/c9dsmfb.

plaques (Fig. 2e, f), microglia morphology (Fig. 2g, h), inflammatory factors (Fig. 2i) and cognitive performance in object-place recognition (Fig. 2j, k) and Morris-water maze tests (Fig. 2l–n).

In addition, taken into consideration potential compensatory effect mediated by other receptors that appear to be indirectly regulated by capsaicin, like TRP channels TRPA1, TRPV2 and voltage-gated ion channels Nav1.7, Kv7.4[28–30], we measured the mRNA levels of these genes, but found significant influence neither by TRPV1 KO nor capsaicin treatment (Supplementary Fig. S5).

Altogether, these results suggest that TRPV1 is not indispensable for the observed protective effects against AD of oral capsaicin treatment.

Gut microbes contribute to the protective effects of capsaicin

Given that gut microbiota has been widely-recognized to be involved in the AD pathogenesis[31], we next investigated the impact of capsaicin on gut microbes in 5×FAD mice. Metagenome sequencing of intestinal contents was performed, and non-redundant gene set was acquired with the similarity threshold at 95% and coverage threshold at 90%. Principal-component analysis (PCA) based on the taxonomic species revealed distinct clustering patterns among samples from vehicle and capsaicin-treated 5×FAD mice (Fig. 3a). 5×FAD mice showed reduction in alpha diversity of microbiota taxonomy, which was reversed by capsaicin, as indicated by increase in the abundance-based coverage estimator (ACE) index (Fig. 3b). In specific, capsaicin predominantly increased the abundance of *Firmicutes* (also known as *Bacillota*), and decreased the abundance of *Bacteroidetes, Proteobacteria* and *Verrucomicrobia* at the phylum level in 5xFAD mice (Fig. 4c). Utilizing the linear discriminant analysis effect size (LEfSe) method, we found many featured species, including several belong to genus of the *Alistipes*, *Oscillibacter, Prevotella, Hungatella*, etc. enriched in the capsaicin-treated group (Fig. 3d).

To examine whether the protective effects of capsaicin were mediated through its modulation on gut microbiota, we performed gut microbiota transfer (GMT) from 5-month 5xFAD mice receiving 1-month capsaicin treatment to a new batch of 5-month 5xFAD mice. Contents from both small intestines and colon were collected to maximize gut microbe enrichment and minimize interference from environmental bacteria in the housing conditions and prevent the disruption of anaerobic bacteria by oxygen exposure. Gut contents from Veh- or Cap-fed 5xFAD mice were collected and immediately processed under anaerobic conditions. Given the low water solubility of capsaicin, all samples underwent repeated washing with pre-reduced PBS followed by centrifugation. The supernatant was obtained and further extracted with oil to remove any potential residual capsaicin. It was confirmed that the Cap was virtually undetectable in the final aqueous phase containing the gut microbes (Fig. 3e, f). The final processed solution was used for GMT in 5-month 5xFAD mice (0.5 mL each day, once every other day for a month), equal doses of PBS was delivered as control (Fig. 3g).

We found that GMT from Cap-treated mice, but not from Veh, significantly reduced Aβ plaques density while inhibiting microglia activation (Fig. 3h–k), and downregulated inflammatory factors in the hippocampus (Fig. 3l). Consistently, GMT from Cap-treated mice improved cognitive functions of 5xFAD mice compared with Veh-GMT and PBS controls in both object-place recognition and Morris-water maze tests (Fig. 3m–p). These results supported a pivotal contribution of the gut microbiota in mediating the amelioration of AD phenotypes by oral capsaicin intake.

Depletion of gut microbes diminishes the beneficial effects of capsaicin

To further ascertain the contribution of gut microbes to the capsaicin's protective effects, we applied high-dose cocktail of antibiotics (ABX) to deplete the gut microbes of either Veh- or Cap-treated 5×FAD mice at 5-month of age. ABX was pretreated through oral gavage every day for 7 days before capsaicin administration and persisted throughout the experiment. The elimination of gut microbes by ABX was confirmed by bacteria culturing (Supplementary Fig. S6a–c). We found in both WT and 5xFAD mice that ABX hindered the cognitive-improving effect of capsaicin (Supplementary Fig. S6d-e). Intriguingly, for 5xFAD mice, ABX alone reduced Aβ plaques and insoluble $A\beta_{42}$, as well as downregulated levels of microglia activation and inflammatory factors in the hippocampus (Supplementary Fig. S6f–k), potentially thanks to the prevention of gut dysbiosis and reduction of harmful metabolites following pan-elimination of gut microbes[32]. Notably, the depletion of gut microbes by ABX nearly abolished the beneficial effects of capsaicin in reducing Aβ aggregates in the brain, and eliminated the anti-inflammatory effects of capsaicin by increasing microglia activation and pro-inflammatory factors levels (Supplementary Fig. S6f–k), suggesting a pivotal contribution of gut microbiota in the anti-AD effects of capsaicin.

https://doi.org/10.1038/s41467-026-68937-9

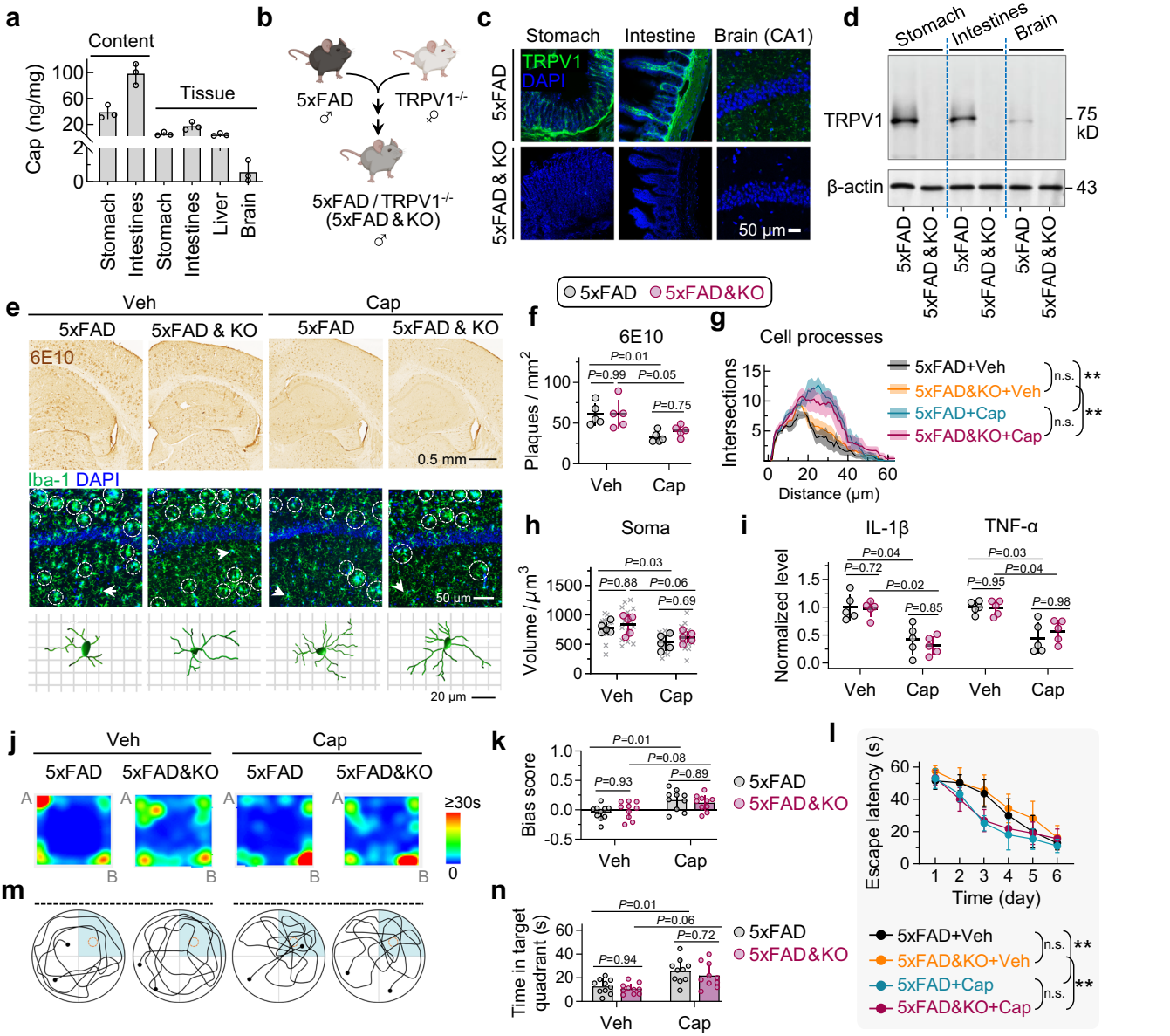

Fig. 2 | TRPV1 knock-out in 5×FAD mice has nonsignificant effect on the capsaicin-mediated amelioration in AD pathologies. a Distribution of capsaicin in digestive tracts and different tissues of 5×FAD mice following repeated administration. $n = 3$ mice in each group. Data are presented as mean ± SD. **b** A cartoon showing the breeding scheme of 5×FAD & TRPV1$^{-/-}$ (KO) mice. Created in BioRender. Zheng, J. (2026) https://BioRender.com/c9dsmfb. **c**, **d** Representative immunofluorescent images and blots showing the expression and knock-out of TRPV1 in different tissues. (**e**–**h**) TRPV1 KO in both veh- and cap-treated 5×FAD mice did not significantly change Aβ plaques (**f**), microglia soma volume (**g**) and cell processes complexity (**h**). White circles in representative images indicate plaque-surrounded cell aggregates, arrows point to cells showed in 3D-reconstruced images (**e**). Crosses indicate individual cells and circles indicate mean values of individual mouse (**h**). Bands indicate SD (**g**). $n = 5$ mice or 15 cells in each group. Data are presented as mean ± SD. Two-way ANOVA followed by Tukey's multiple comparisons test. Statistics of panel (**g**): 5×FAD+Veh vs 5×FAD&KO+Veh, $P = 0.79$ (n.s.); 5×FAD+Cap *vs* 5×FAD&KO+Cap, $P = 0.98$ (n.s.); 5×FAD +Veh *vs* 5×FAD+Cap, $^{**}P = 0.0002$; 5×FAD&KO+Veh vs 5×FAD&KO+Cap, $^{**}P = 0.01$. **i** TRPV1 KO induced nonsignificant change in inflammatory factors, and did not alter the effect of capsaicin on downregulating IL-1β and TNF-α. Data were normalized by the mean value of Veh+5×FAD group for each inflammatory factor. $n = 5$ mice in each group. Data are presented as mean ± SD. Two-way ANOVA followed by Tukey's multiple comparisons test. **j**,**k** TRPV1 KO neither change the baseline object-place recognition of 5xFAD mice, nor abolish the cognitive-improving effect of capsaicin. Representative heatmaps (**j**) showed the time distribution of mice spent in test chambers. $n = 10$ mice in each group. Data are presented as mean ± SD. Two-way ANOVA followed by Tukey's multiple comparisons test. TRPV1 KO had limited effects on baseline spatial learning (**l**) and memory (**n**) of 5xFAD mice, and did not cancel the cognitive-enhancing effects of capsaicin in Morris-water maze test. Representative images showed the trajectories of mice swimming in the water maze during the test phase, and cyan areas indicate the target quadrant in water maze (**m**). $n = 10$ mice in each group. Data are presented as mean ± SD. n.s. non-significant, repeated measures (**l**) or two-way (**n**) ANOVA followed by Tukey's multiple comparisons test. Statistics of panel (**l**): 5×FAD+Veh vs 5×FAD&KO+Veh, $P = 0.10$ (n.s.); 5×FAD+Cap *vs* 5×FAD&KO+Cap, $P = 0.70$ (n.s.); 5×FAD +Veh *vs* 5×FAD +Cap, $P = 0.0002^{**}$; 5×FAD&KO+Veh *vs* 5×FAD&KO+Cap, $P = 0.0001^{**}$. Source data are provided as a Source Data file.

Gut microbiota regulates 24-hydroxycholesterol level in 5×FAD mice under capsaicin treatment

To investigate how the capsaicin-induced gut microbiota remodeling mediated the observed protective effects against AD, we performed further analysis of differentially expressed metagenomic gene sets in capsaicin-treated 5×FAD mice, and found the top-2 enriched pathways of the gene sets as glycan and lipid metabolism (Fig. 4a, b). Subsequently, we examined metabolic profile in the plasma of 5×FAD mice

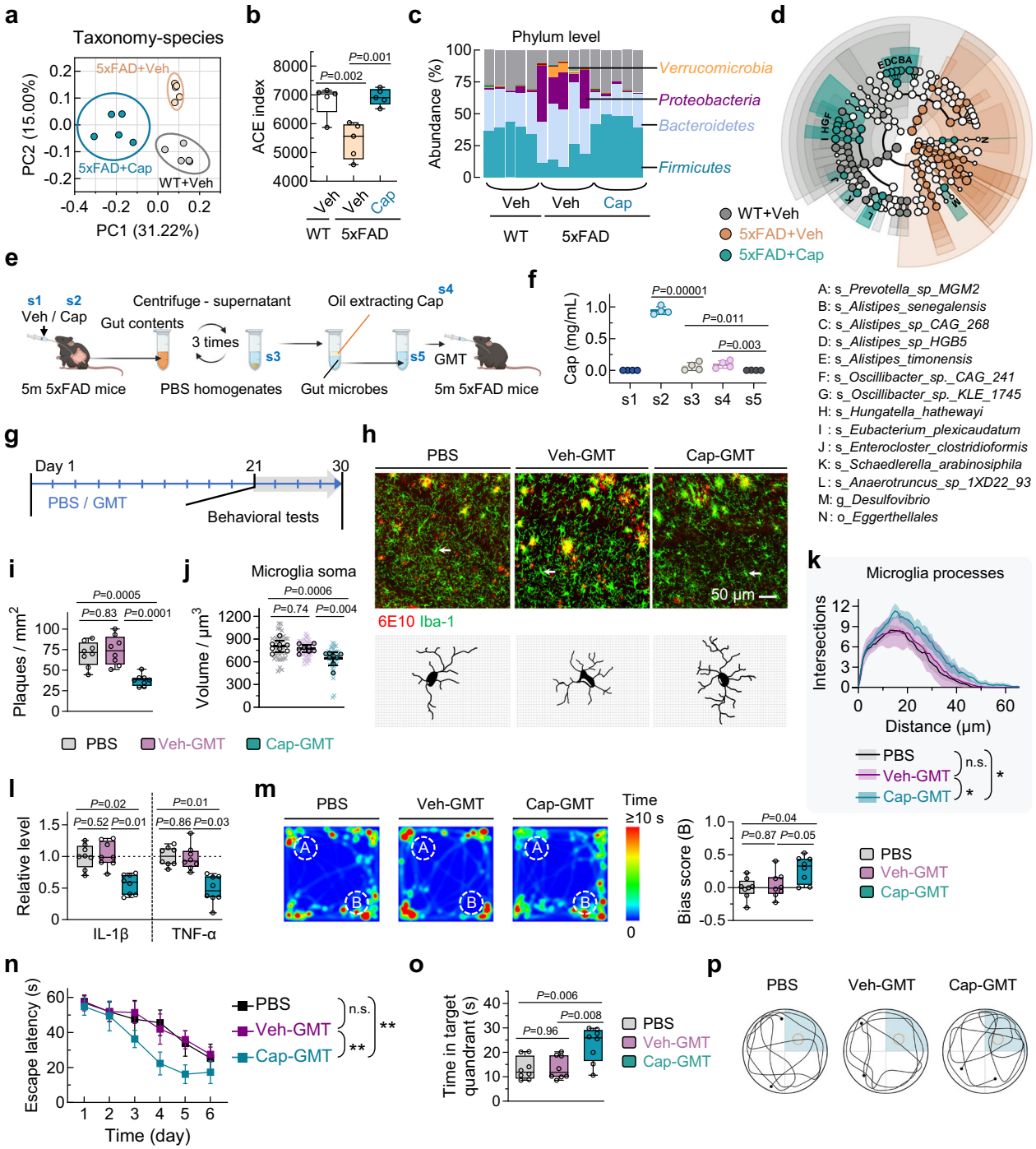

following repeated capsaicin treatment (Fig. 4c, d, Supplementary Data 5), and found that different metabolites were predominantly involved in lipid metabolism-associated pathways (Fig. 4e, Supplementary Data 6). Specifically, we noted that capsaicin downregulated the level of cholesterol while upregulated its derivate 24(S)-hydroxycholesterol (24-HC, also known as cerebrosterol) (Fig. 4d, f), the latter has been revealed to be capable of alleviating cognitive deficits and reducing Aβ burden[33,34], but traditionally considered to be specifically synthesized from cholesterol in central nervous system by CYP46A1[35].

Thereby, we measured whether pan depletion of gut microbiota ABX affects 24-HC levels by liquid chromatography mass spectrometry (LC-MS) in the gut contents, plasma and hippocampus of WT and 5xFAD mice. Firstly, 5xFAD mice had dominantly lower levels of 24-HC in all those detected samples compared with WT mice. For both WT and 5xFAD mice, capsaicin treatment upregulated 24-HC levels in the intestinal contents, plasma and hippocampus, which were all reversed by the depletion of gut microbes with ABX. Especially, in the intestinal contents, ABX almost brought down the level of 24-HC to nil, suggesting a contribution of gut microbiota in the capsaicin-induced upregulation of 24, especially in the peripheral (supplementary Fig. S7a-b).

Additionally, we examined whether the reduction of 24-HC at different levels were resulted from potential inhibition of 24-HC synthesis in the brain by ABX, both mRNA and protein levels of CYP46A1 in the brain were measured. It was found that CYP46A1 was downregulated in 5xFAD mice compared with WT mice, suggesting that the central production of 24-HC in AD was also downregulated in

Fig. 3 | Gut microbiota contributes to the amelioration of AD phenotypes by oral capsaicin intake in 5×FAD mice. a PCA of gut microbe species of indicated groups. $n = 5$ mice in each group. **b** Capsaicin reversed the reduction of ACE index in 5×FAD mice. $n = 5$ mice in each group. Data are presented as box and whiskers, min-max. One-way ANOVA followed by Tukey's multiple comparisons tests. **c** Relative abundance of microbiota at the phylum level in indicated groups. **d** Taxonomic cladogram of intestinal bacteria to species level revealed by LEfSe analysis. Cyan bands and dots indicate featured bacteria with featured enrichment in capsaicin-treated 5×FAD mice. **e**,**f** Experimental scheme of gut microbe isolation and validation of capsaicin removal from gut microbiota transfer (GMT) samples. $n = 4$ pooled samples in each group. Data are presented as mean ± SD. One-way ANOVA followed by Tukey's multiple comparisons tests. Illustrative components in panel e are created in BioRender. Zheng, J. (2026) https://BioRender.com/c9dsmfb. **g** Experimental schedule of GMT. Phosphate buffered saline (PBS) was used as control. **h**–**k** GMT from Cap-treated mice decreased density of Aβ plaques (**i**) and microglia soma volume (**i**), and increased microglia processes branching complexity (**k**) in the hippocampal CA1 of 5xFAD mice. Arrows in presentative images (**h**) indicate cells showed in reconstructed images (lower panels). Crosses represent individual cells and circles indicate mean value of each mouse (**j**). Bands indicate SD (**k**). $n = 40$ cells from 8 mice in each group. Data are presented as box and whiskers, min-max (**i**) or mean ± SD (**j**, **k**). n.s. nonsignificant, one-way (**i**, **j**) or two-way (**k**) ANOVA followed by Tukey's multiple comparisons tests. Statistics in panel k: PBS vs Veh-GMT, $P = 0.893$; Veh-GMT *vs* Cap-GMT, $P = 0.042$*; PBS vs Cap-GMT, $P = 0.038$*. **l** GMT from Cap-treated mice downregulated pro-inflammatory levels in the hippocampus tissue. $n = 8$ mice in each group. Data were normalized to the mean value of PBS group. Data are presented as box and whiskers, min-max. Two-way ANOVA followed by Tukey's multiple comparisons tests. GMT from Cap-treated mice improved object-place recognition (**m**), and spatial learning (**n**) and memory (**o**, **p**) in the Morris-water maze test of 5xFAD mice. Cyan areas indicate the target quadrant in water maze (**p**). $n = 8$ mice in each group. Data are presented as box and whiskers, min-max (**m**, **o**) or mean ± SD (**n**). One-way (**m**, **o**) or repeated measures (**n**) ANOVA followed by Tukey's multiple comparisons tests. Statistics in panel n: PBS vs Veh-GMT, $P = 0.901$ (n.s.); Veh-GMT vs Cap-GMT, $P = 0.0001$**; PBS vs Cap-GMT, $P = 0.0001$**. Source data are provided as a Source Data file.

the brain of AD mice aside from gut. Nonetheless, CYP46A1 expression in the brain was affected neither by capsaicin nor ABX treatment (Supplementary Fig. S7c–e).

Gut *Oscillibacter* is involved in the production of 24-HC

Next, we sought to investigate whether 24-HC can be synthesized in the gut in a microbiome-dependent way. Combinative analysis of metagenomic and metabolomic data revealed that the level of 24-HC metabolism had most predominantly positive correlation with the *Oscillibacter* genus belonging to the *Oscillospiraceae* family in *Firmicutes* phylum (Fig. 4g), which was revealed to be capable of metabolizing cholesterol to generate hydroxycholesterol, presumed to depend on the expression of ismA homologous gene[17,20]. Thus, we next focused on the regulation of 24-HC by *Oscillibacter*. Further analysis of metagenomic data revealed reduced abundance of several belonging species and the overall *Oscillibacter* genus in 5xFAD mice, which was significantly rescued by capsaicin treatment (Fig. 4h, i). Meanwhile, the *Oscillibacter* abundance correlated negatively with plasma cholesterol level and positively with 24-HC level in liner regression analysis (Fig. 4j).

Furthermore, we examined *Oscillibacter* changes in AD patients in GMrepo v2, a curated human gut microbiome database[36]. In one of the three AD datasets included[37–39], namely dataset PRJNA770746, a significant enrichment of *Oscillibacter* in healthy controls was found (LDA score = −3.17). Overall, the abundance of *Oscillibacter* was significantly downregulated in AD patients compared with healthy controls (Fig5a-b). Besides, one previous case study found that sustained treatment of in vitro cultured human feces with capsaicin led to a significant increase in *Oscillibacter* abundance[40]. Collectively, these findings suggest a potential link between dietary capsaicin intake with increase in gut *Oscillibacter* abundance.

Next, we isolated gut microbes under anaerobic conditions from Cap-treated 5xFAD mice, and identified *Oscillibacter* via whole-genome sequencing (Fig. 5c). The isolated *Oscillibacter* was further validated by prominent expression of preciously reported marker genes including Oscillibacter-specific 16S rRNA (V3-V4 region), ismA and CgT homologous genes[17], as measured by qPCR compared with negative controls of *E.coli* and positive control of J115 (Fig. 5d). Besides, we ascertained the capacity of *Oscillibacter* to generate 24-HC in cultures. Cholesterol treatment for 24 h significantly increased the 24-HC level in the culture medium, which was further upregulated under capsaicin co-administration (Fig. 5e). Subsequently, we grafted *Oscillibacter* repeatedly into 5-month 5xFAD mice for a month, equal doses of culture medium were inoculated as control (Fig. 5f). The results showed that *Oscillibacter* supplement significantly reduced Aβ plaques density (Fig. 5g), inhibited microglia overactivation while downregulating pro-inflammatory factors levels (Fig. 5g–k), and improved cognitive functions of 5xFAD mice (Fig. 5l–o). These outcomes mimicked the protective effects of oral capsaicin intake.

Taken together, these data suggest the existence of peripheral production of 24-HC, and a pivotal contribution of gut *Oscillibacter* as well as modulatory effect of capsaicin in this process.

24-HC facilitates microglia phagocytosis of Aβ and suppresses inflammation

To examine whether and how 24-HC affects microglia overactivation and Aβ phagocytosis, increasing doses of 24-HC were administrated in BV2 cells, a mouse-derived microglia cell line. Limited cytotoxicity of 24-HC was observed at concentrations lower than 50 μM in the MTT assay (supplementary Fig. S8a). In subsequent, Rhodamine B (RhB)-conjugated Aβ was added in LPS pre-treated BV2 cell cultures. After wash-out of extracellular Aβ in the medium, we found that 24-HC at 10 μM significantly increased the amount of Aβ phagocytized by BV2 cells at 4.5 h post administration, and upregulated clearance rate of phagocytized Aβ (intracellular Aβ: (4.5 h −24 h) / 4.5 h) (Fig. 6a–c). The facilitation of Aβ phagocytosis in the 24-HC-treated group was also confirmed by increased portion of Aβ-containing cells at 4.5 h (Fig. 6d). Furthermore, 24-HC at 10 μM also significantly reversed the Aβ-induced upregulation of pro-inflammatory factors IL-1β and TNF-α (Fig. 6e), increased percentage of BV2 cells expressing CD206 that were traditionally recognized to have high phagocytic and low pro-inflammatory activities, as well as decreased percentage of cells expressing CD16/32 and CD86, which are recognized to be highly pro-inflammatory and aggressive[41] (Supplementary Fig. S8b–e). Consistently, the effects of 24-HC in facilitating Aβ phagocytosis and downregulating inflammatory factors at 10 μM were also observed in primary cultured mouse microglia (Supplementary Fig. S8f–h).

Next, we tested how direct supplement of 24-HC in 5-month-old 5×FAD mice affected microglia function and Aβ deposition in the brain. 24-HC was intraperitoneally (i.p.) injected once every other day (0.01 mg/kg, dissolved in DMSO) for a consecutive month, which significantly elevated the level of 24-HC in the hippocampus (Fig. 6f–g), indicating that peripheral 24-HC can at least partly cross the brain-blood barrier (BBB). To further confirm the 24-HC absorption in gut tracts and its penetrability across the BBB, we conjugated 24-HC with fluorescein BODIPY-FL and administrated the 24-HC-BODIPY-FL (0.02 mg/kg, i.g.) in 5-month-old 5xFAD mice for consecutively 7 days. Prominent fluorescent signals were detected in homogenates of gut contents, intestines, plasma and hippocampus tissue, respectively, though the percentage of labeled 24-HC reaching the brain appeared to remain much lower than those in guts and blood after treatment, which was possibly due to rapid metabolism in the liver and other peripheral organs. Moreover, to rule out potential interference from fluorescein on the membrane-penetrating efficiency of 24-HC, we also

https://doi.org/10.1038/s41467-026-68937-9

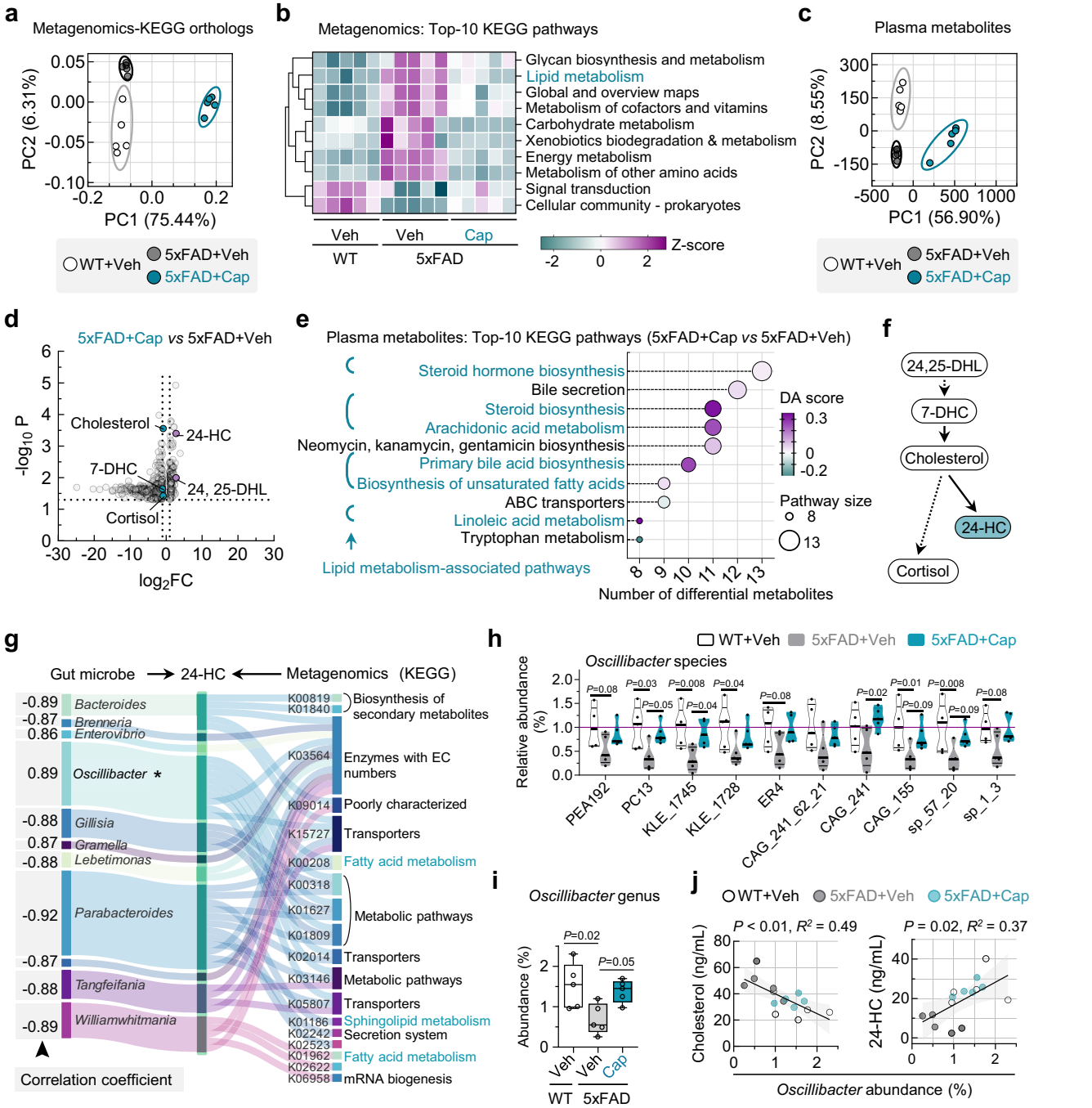

Fig. 4 | Elevation of 24-HC level associates with increase in gut Oscillibacter in 5×FAD mice following capsaicin treatment. a PCA based on KEGG functional gene sets in metagenome for indicated groups. $n = 5$ mice in each group. **b** Top-10 enriched KEGG pathways of differentially expressed metagenomic gene sets between cap- and veh-treated 5×FAD mice. **c** PCA based on plasma metabolites of indicated groups. $n = 5$ mice in each group. **d** Metabolites with significant changes between cap- and veh-treated 5×FAD mice. Two-sided Mann–Whitney U tests with P-values corrected using the Benjamini-Hochberg method. **e** Top-10 enriched KEGG pathways of different metabolites between cap- and veh-treated 5×FAD mice. Pathways highlighted in cyan fonts indicate lipid metabolism-associated pathways. DA, Differential abundance. **f** A traditional metabolic pathway in the brain for cholesterol to generate 24-HC. 24, 25-DHL, 24,25-dihydroxycholecalciferol. 7-DHC, 7-dehydrocholesterol. **g** Correlation among gut microbe genera with top-10 coefficient score, 24-HC level and bacterial KEGG gene sets. Stars indicate the two bacteria genera showing highest correlation coefficient with 24-HC, respectively. Capsaicin partly rescued the downregulation of gut *Oscillibacter* abundance in 5xFAD mice in many species (**h**) and at the overall genus level (**i**). $n = 8$ mice in each group. Data are presented as median with quartiles (**h**), or box and whiskers, min-max (**i**). Two-way (**h**) or one-way (**i**) ANOVA followed by Tukey's multiple comparisons tests. **j** *Oscillibacter* abundance negatively correlated with plasma cholesterol level, while positively correlated with 24-HC level. Linear regression analysis, gray bands indicate 95% confidence interval. Source data are provided as a Source Data file.

https://doi.org/10.1038/s41467-026-68937-9

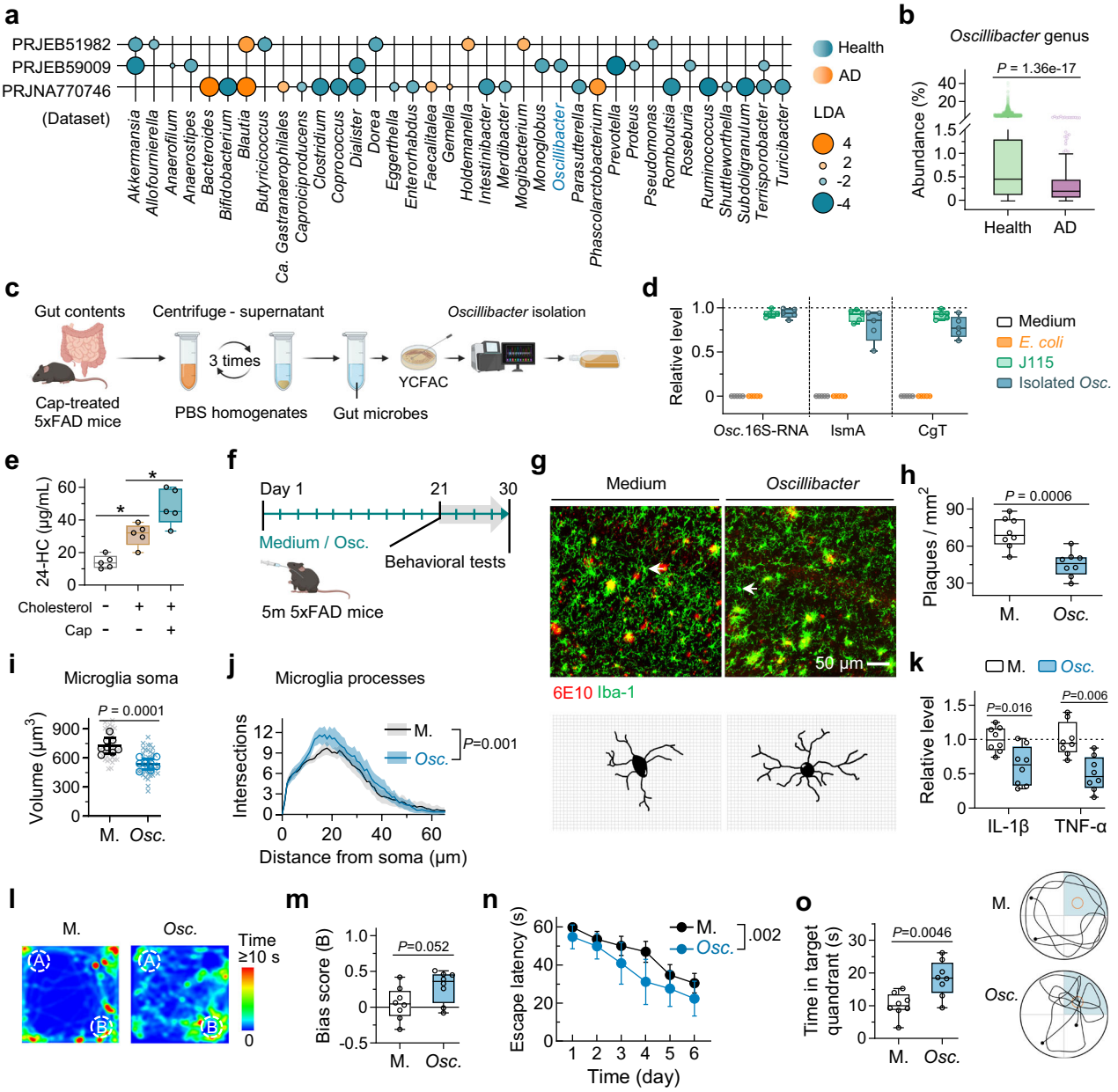

Fig. 5 | Direct introduction of *Oscillibacter* alleviates Aβ-related AD pathologies in 5xFAD mice. a Featured enrichment of gut microbes at genus level, including *Oscillibacter*, in healthy individuals versus AD patients recorded in GMrepo v2 database. Linear discriminant analysis (LDA) scores were acquired using LEfSe analysis. **b** AD patients showed significantly decreased *Oscillibacter* abundance compared with healthy group. $n = 15{,}780$ (healthy) or 218 (AD). Data are presented as box and whiskers, Tukey. Two-sided Mann–Whitney U test. **c** Experimental procedures of *Oscillibacter* isolation from gut contents of Cap-treated 5xFAD mice. **d** Isolated *Oscillibacter* (*Osc.*) showed high expression levels of *Osc.*-specific 16S rRNA, ismA and CgT homologous genes relative to the level of pan bacterial 16S rRNA. $n = 5$ dishes per group. Culture medium and *E. coli* were used as negative control. J115 was used as positive control. Data are presented as box and whiskers, min-max. **e** 24-HC level in the culture medium of *Oscillibacter* was upregulated following cholesterol treatment, and further increased under Cap co-treatment. $n = 5$ dishes per group. Data are presented as box and whiskers, min-max. One-way ANOVA followed by Tukey's multiple comparisons tests. **f** Experimental scheme of medium and *Oscillibacter* delivery in 5xFAD mice. **g**–**j** Direct *Oscillibacter* grafting decreased Aβ plaques density (**h**), decreased the soma volume (**i**) and increased cell processes branching complexity (**j**) of microglia in the hippocampal CA1 of 5xFAD mice compared with medium (M.). Arrows in presentative images (**g**) indicate microglia showed in reconstructed images (lower panels). Crosses indicate individual cells and circles indicate mean values of individual mouse (**i**). Bands indicate SD (**j**). $n = 40$ cells from 8 mice in each group. Data are presented as box and whiskers, min-max (**h**, **k**), or mean ± SD (**i**, **j**). Two-sided unpaired *t* tests (**h**, **i**) or two-way ANOVA (**j**). **k** *Oscillibacter* downregulated pro-inflammatory levels in the hippocampal tissue. $n = 8$ mice in each group. Data were normalized to the mean value of medium group. Data are presented as box and whiskers, min-max. Two-way ANOVA followed by Tukey's multiple comparisons tests. **l**,**m** *Oscillibacter* improved object-place recognition of 5xFAD mice. $n = 8$ mice in each group. Data are presented as box and whiskers, min-max. Two-sided unpaired *t* test. *Oscillibacter* improved spatial learning (**n**) and memory (**o**) of 5xFAD mice in the Morris-water maze test. Cyan areas indicate the target quadrant in water maze (**o**). $n = 8$ mice in each group. Data are presented as mean ± SD (**n**), or box and whiskers, min-max (**o**). Two-way ANOVA (**n**) or two-sided unpaired *t* test (**o**). Source data are provided as a Source Data file. Illustrative components in panels (**c** and **f**) are created in BioRender. Zheng, J. (2026) https://BioRender.com/c9dsmfb.

https://doi.org/10.1038/s41467-026-68937-9

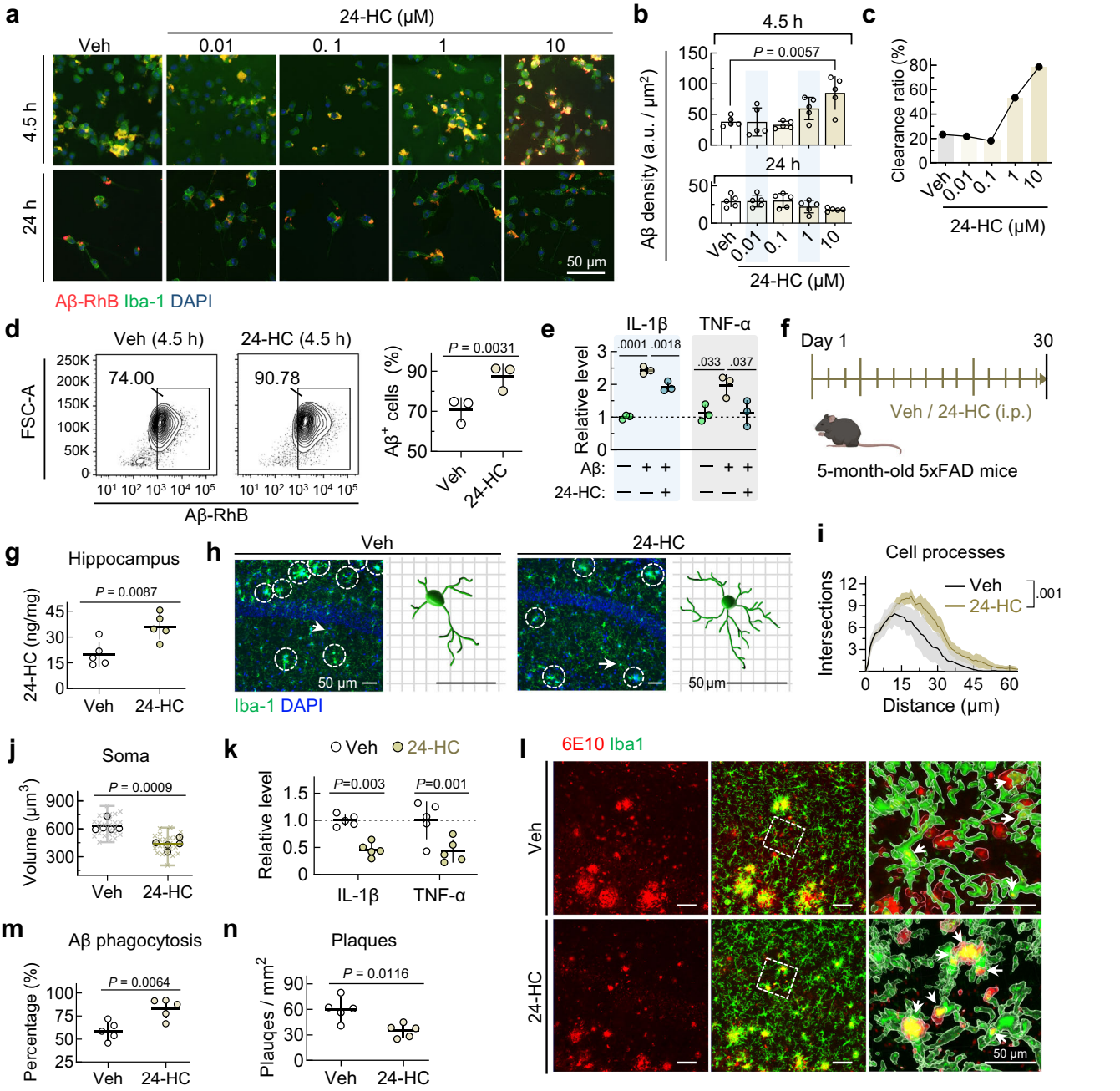

Fig. 6 | 24-HC suppresses microglia overactivation and promotes Aβ phagocytosis. a, **b** 24-HC at 10 μM increased the amount of Aβ phagocytized by BV2 cells at 4.5 h, but not 24 h post administration. $n = 5$ cell wells in each group. Data are presented as mean ± SD. One-way ANOVA followed by Tukey's multiple comparisons tests. **c** The mean Aβ clearance ratio was highest at the 10 μM dose of 24-HC. **d** 24-H increased the percentage of Aβ-containing BV2 cells at 4.5 h. Data were collected from 9 wells of cell and 3 batches of experiments per group. Data are presented as mean ± SD. Two-sided unpaired *t* tests. **e** 24-HC co-administration inhibited the Aβ-induced increase in IL-1β and TNF-α levels. $n = 3$ cell wells in each group. Data are presented as mean ± SD. One-way ANOVA followed by Tukey's multiple comparisons tests. **f** Experimental diagram illustrating 24-HC or vehicle treatment in 5×FAD mice. Certain illustrative components are created in BioRender. Zheng, J. (2026) https://BioRender.com/c9dsmfb. **g** 24-HC supplement upregulated the 24-HC level in the hippocampus of 5×FAD mice. $n = 5$ mice in each group. Data are presented as mean ± SD. Two-sided unpaired *t* test. **h**–**j** 24-HC decreased microglia processes complexity (**i**) and soma volume (**j**) in the hippocampus. White circles in representative images indicate plaque-surrounded microglia aggregates, arrows point to the cell showed in 3D-reconstructed images. Bands indicate SD (**i**). Crosses indicate individual cells and circles indicate mean values of individual mouse (**j**). $n = 20$ cells from 5 mice in each group. Data are presented as mean ± SD. Two-way ANOVA (**i**) or two-sided unpaired *t* tests (**j**). **k** 24-HC downregulated IL-1β and TNF-α levels in the hippocampus. Data were normalized to the mean value of Veh groups. $n = 5$ mice in each group. Data are presented as mean ± SD. Two-way ANOVA followed by Tukey's multiple comparisons tests. **l**–**n** 24-HC increased the portion of Aβ phagocytized by microglia (**m**), and decreased the overall density of Aβ plaques (**n**) in the hippocampus. White boxes in representative images indicate the area showed in 3D-reconstructed images on right, arrows point to representative sites of Aβ phagocyted by microglia (**l**). $n = 5$ mice in each group. Data are presented as mean ± SD. Two-sided unpaired *t* tests. Source data are provided as a Source Data file.

administrated equal doses of natural 24-HC in 5xFAD mice, and still measured elevation of 24-HC in these regions (Supplementary Fig. S9).

In consistent with findings in in vitro experiments, 24-HC supplement significantly suppressed the overactivation of microglia and inflammation level in the hippocampus of 5×FAD mice, as indicated by decrease in microglia soma volume, increase in cell processes complexity, and reduction in proinflammatory factors IL-1β and TNF-α (Fig. 6h–k). Moreover, 3D-reconstruction of co-immunostaining images showed that 24-HC increased the percentage of Aβ phagocytized by microglia, along with overall decrease in Aβ plaques (Fig. 6l–n). Altogether, these results suggest that 24-HC suppressed microglia overactivation and promoted Aβ phagocytosis.

In addition, to determine whether central synthesis of 24-HC in the brain was necessary for the alleviation of AD-related pathologies under peripheral 24-HC supplement, we treated 5xFAD mice with soticlestat (SOT) (50 mg/kg, i.g.), an inhibitor of CYP46A[42], in combination with peripheral supplement of vehicle / 24-HC for consecutively 30 days. SOT significantly reduced 24-HC levels in the hippocampus and plasma, but did not affect intestinal 24-HC level. Notably, oral 24-HC supplementation was still effective in increasing hippocampal 24-HC levels even under SOT co-administration (Supplementary Fig. S10a-b). For AD pathologies, SOT alone increased Aβ plaque deposition in the hippocampus, while combined treatment with 24-HC partially, but not completely, counteracted 24-HC's ability to reduce Aβ burden (Supplementary Fig. S10c-d). Interestingly, SOT did not further exacerbate microglial activation in 5xFAD mice, likely due to a ceiling effect, yet it still upregulated hippocampal IL-1β levels, both alone and in combination with 24-HC (Supplementary Fig. S10c, e–g). Furthermore, SOT significantly impaired 24-HC's beneficial effect on object-place recognition (Supplementary Fig. S10h-i). These results suggest that 24-HC synthesis in both the brain and gut plays a crucial role in mitigating brain pathologies.

24-HC targets on LXRβ to suppress microglia overactivation and inflammation

To determine molecular mechanisms mediating the 24-HC's beneficial effects, we measured several proteins that has been recognized to directly bind 24-HC, including liver x receptor (LXR) α / β and retinoid-related orphan receptor gamma (RORγ), all of which are ligand-regulated nuclear receptors that are capable of translocating from cytoplasm into cell nucleus to regulate inflammatory gene transcription[43,44]. We found that at 4.5 h following 24-HC administration in BV2 cells, the nuclear / cytosol distribution ratio of only LXRβ, but not LXRα and RORγ, was significantly increased (Fig. 7a–c). Furthermore, in the nuclear fraction of both BV2 cells and primary cultured microglia, 24-HC elevated the SUMOylation level of LXRβ (Fig. 7d, supplementary Fig. S11a), which were previously revealed to be critical for LXRβ to play as a transcriptive suppressor of inflammatory genes[45,46]. Meanwhile, the heterocomplex formation of LXRβ with transcriptional corepressors nuclear factor-kappa B (NF-κB) p65 and p50 was suppressed (Fig. 7e).

We sought to evaluate whether LXRβ in microglia was indispensable for the anti-inflammatory effect of 24-HC, through applying siRNA to downregulate the expression of LXRβ by 45.67% in BV2 cells (Fig. 7f). At 4.5 h following Aβ co-administration, 24-HC significantly decreased levels of IL-1β and TNF-α (Fig. 7g), decreased ratio of $CD16/32^{+}$ to $CD206^{+}$ cell portion (Fig. 7h, i), and promoted Aβ phagocytosis (Fig. 7j) in BV2 cells transfected with control vectors, while all these anti-inflammatory effects of 24-HC were nearly abolished under LXRβ knock-down (Fig. 7g–j), suggesting a pivotal role of LXRβ in mediating the anti-inflammatory effect of 24-HC on microglia.

Next, we accessed whether the observed protective effects of capsaicin in 5×FAD mice were dependent on LXRβ. In consistent with BV2 cells, capsaicin treatment in 5×FAD mice also increased the SUMOylation level of LXRβ in the nuclear fraction of hippocampal tissue (supplementary Fig. S11b). To selectively knock down LXRβ in hippocampal microglia, we stereotaxically infused adeno-associated virus AAV-CMV-DIO-shLXRβ-EGFP into 5×FAD / Cx3cr1-CreERT2 mice at 5-month of age. AAV-CMV-DIO-EGFP was injected as control (Fig. 7k). The AAV MG1.2 variant was used since it can mediate sufficient transgene expression in microglia without inducing immune activation[47]. The efficiency and specificity of LXRβ knock-down in microglia were confirmed through high co-labeling percentage of EGFP / Iba1 (Fig. 7l, supplementary Fig. S11c), prominent decrease in LXRβ immunoreactivity in microglia, and exclusive downregulation of LXRβ mRNA level in AAV-shLXRβ-infected cells (supplementary Fig. S11d-e). Following long-term 24-HC treatment, we found that conditional knock-down of LXRβ in hippocampal microglia significantly aggravated microglia activation (Fig. 7m–o), suppressed Aβ-phagocytosis (Fig. 7m, p), increased Aβ plaques amounts (Fig. 7q), as well as upregulated levels of IL-1β and TNF-α (Fig. 7r).

Altogether, these results suggest that 24-HC inhibits microglia overactivation and promote Aβ phagocytosis through enhancing the transcriptive suppression of LXRβ on inflammatory factors (Fig. 7s).

Capsaicin upregulates 24-HC and alleviates AD-like tau pathology in P301S mice

Given that abnormal microglia activation and inflammation were also important drivers of tau hyperphosphorylation and aggregation[48,49], another set of pathologic hallmarks in AD patients, we next sought to examine any potential therapeutic effects of capsaicin intake in 5-month-old P301S mice, a transgenic line expressing human 1 N/4 R tau with P301S mutation[50], since tau pathology is not evident in 5×FAD mice. Capsaicin was orally gavaged once a day and consecutively for 40 days throughout the experiment. In similar with 5×FAD mice, P301S mice also showed reduction in 24-HC levels in the intestinal contents, plasma and hippocampus, all of which were partly reversed by capsaicin treatment (supplementary Fig. S12a-b). Consistently, capsaicin upregulated the SUMOylation and total level of LXRβ, as well as decreased morphological signs of microglia activation (supplementary Fig. S12c–g).

Of note, for AD-associated tau pathologies, capsaicin significantly downregulated the levels of paired helical filaments tau (PHF-tau) recognized by the AT8 antibody, and downregulated tau phosphorylation at AD-related epitopes including Thr181 and Thr217. These change in tau might be associated the downregulation of tau kinases activation including CaMKII, p38 and GSK-3β, as indicated by decreased ratios of phosphorylated kinase CaMKII (Thr286), p38 (Thr180 / Tyr182) and GSK-3β (Y216) to total protein, respectively (supplementary Fig. S12h–j). Indeed, all of these tau kinases were previously reported to be activated by microglia activation and neuroinflammation[48,51].

In consistent with the amelioration of the tau hyperphosphorylation, we found that capsaicin increased dendritic spine density of pyramid neurons revealed by Golgi-staining, and increased the density of synaptic connections under electron microscopy within the hippocampus CA1 of P301S (supplementary Fig. S12k–l). Besides, capsaicin also improved mice performance in the object-place recognition test, and improved spatial learning and memory in the Morris-water maze test (supplementary Fig. S12m–q).

To sum up, these results suggest significant effectiveness of oral capsaicin treatment in ameliorating tau-related pathologies in AD.

Elevation of 24-HC level in AD patients with moderate-to-high chili intake correlates with cognitive improvement and lower levels of AD biomarkers

Finally, we accessed 24-HC levels in human plasma of the cohort 2, and found that MCI and AD patients with moderate-to-high capsaicin intake from chili-rich diets had significantly higher 24-HC level o compared with those having no / low chili consumption (Fig. 8a).

https://doi.org/10.1038/s41467-026-68937-9

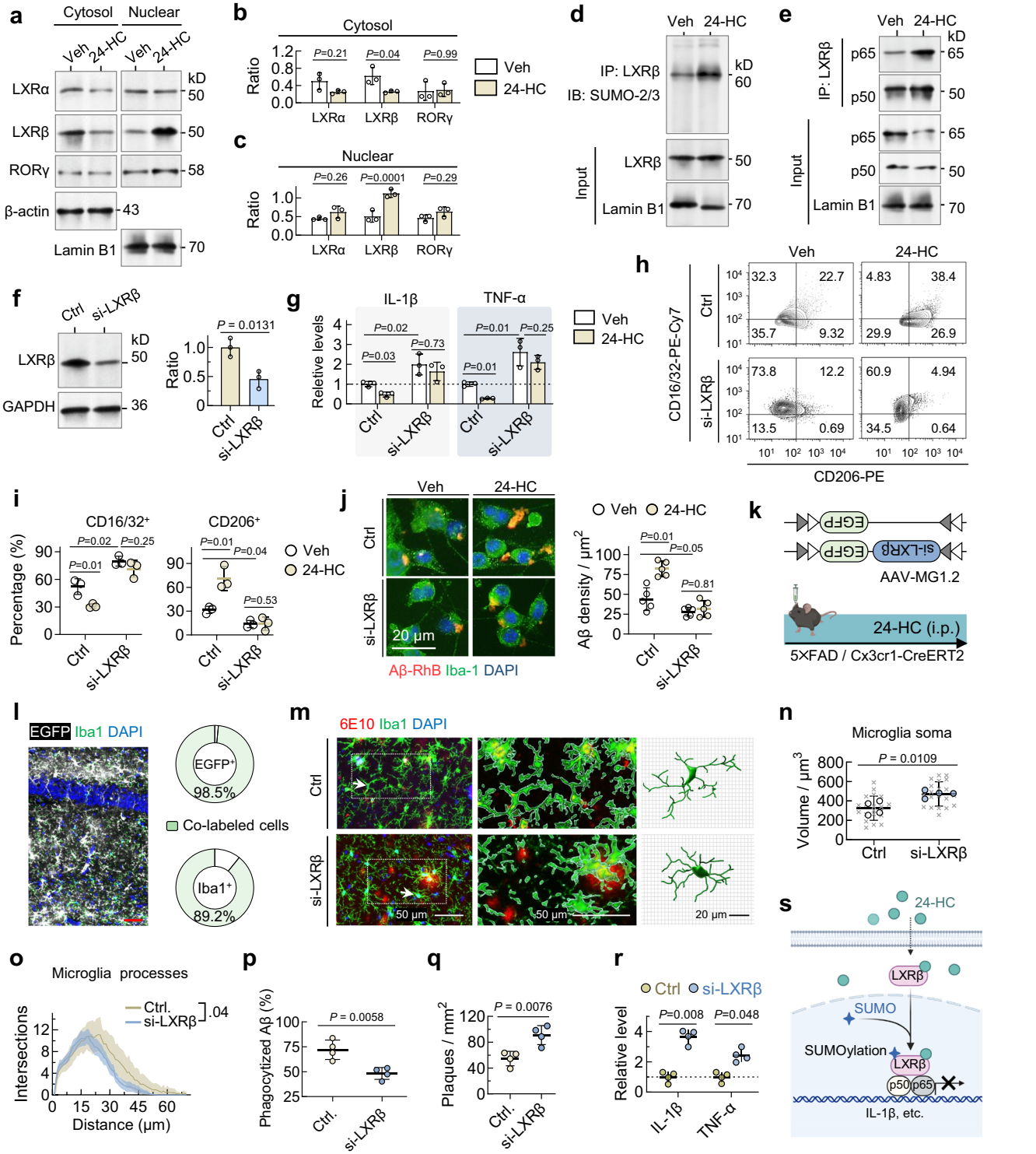

Meanwhile, we also evaluated plasma levels of Aβ42, Aβ40, p-tau181, p-tau217, and neurofilament light chain (NfL) utilizing chemiluminescent enzyme immunoassay (CLEIA)[52]. The group with moderate-to-high capsaicin intake had significantly lower levels of Aβ42 and Aβ40, but higher ratio of Aβ42 to Aβ40, as well as decreases in p-tau181 and p-tau217, though there was nonsignificant change in NfL (Fig. 8b, c). Pearson correlation analysis showed that the plasma 24-HC level positively correlated with the MMSE score, MoCA score and Aβ42 / Aβ40 ratio (Fig. 8d–f), and negatively correlated with the levels of p-tau181 and p-tau217 (Fig. 8g, h). Overall, these data indicate that moderate-to-high capsaicin intake correlated with upregulation in plasma 24-HC and alleviation of AD pathologies in patients.

Discussion

We found in the present study that dietary intake of capsaicin ameliorated AD-related pathologies through promoting gut microbiota-dependent production of 24-HC, the latter targeted LXRβ in the brain to suppress microglia overactivation and inflammation, thereby to facilitate Aβ phagocytosis and clearance, as well as to inhibit tau hyperphosphorylation. The potential protective effects against AD of

https://doi.org/10.1038/s41467-026-68937-9

Fig. 7 | 24-HC targets on LXRβ to suppress microglia overactivation and inflammation. a – **c** 24-HC increased the ratio of nucleus / cytoplasm LXRβ, but did not change LXRα and RORγ in Aβ-treated BV2 cells. $n = 3$ cell wells in each group. Data are presented as mean ± SD. Two-way ANOVA followed by Tukey's multiple comparisons tests. 24-HC increased the SUMOylation level of LXRβ (**d**), and facilitated the formation of LXRβ-p65/p50 hetero-complex (**e**). **f** si-LXRβ down-regulated the protein level of LXRβ in BV2 cells. $n = 3$ wells of cell in each group. Data are presented as mean ± SD. Two-sided unpaired *t* test. **g** si-LXRβ increased IL-1β and TNF-α levels, and abolished the anti-inflammatory effect of 24-HC in BV2 cells co-administrated with Aβ. $n = 3$ wells of cell in each group. Data were normalized to the mean value of control group. Data are presented as mean ± SD. Two-way ANOVA followed by Tukey's multiple comparisons tests. **h,i** si-LXRβ increased the portion of CD16/32-positive BV2 cells while decreased the portion of CD206-positive cells, and abolished the effect of 24-HC in suppressing the pro-inflammatory switch of BV2 cells. $n = 9$ wells of cell and 3 batches of experiments in each group. Data are presented as mean ± SD. Two-way ANOVA followed by Tukey's multiple comparisons tests. **j** si-LXRβ decreased the amount of Aβ phagocytized in BV2 cells, and inhibited the effect of 24-HC in facilitating Aβ phagocytosis. $n = 5$ wells of cell in each group. Data are presented as mean ± SD. Two-way ANOVA followed by Tukey's multiple comparisons tests. **k** Experimental diagram illustrating AAVs injection and 24-HC treatment in 5×FAD / Cx3cr1-CreERT2 mice. **l** Representative image and percentage of AAV-mediated EGFP expression in microglia (in relation to the Supplementary Fig. S11c). **m**–**q** si-LXRβ increased the soma volume (n), decreased cell processes branching complexity (o) of microglia, decreased portion of phagocytized Aβ (p) and increased overall plaques density (q) in the hippocampus under 24-HC. While boxes in representative images (m) indicate the area showed in 3D-reconstrunted images (middle), arrows indicate microglia showed in reconstructed images (right). Crosses indicate individual cells and circles indicate mean values of individual mouse (n). Bands indicate SD (o). $n = 20$ cells from 4 mice in each group. Data are presented as mean ± SD. Two-sided unpaired *t* test (**n**, **p**, **q**) or two-way ANOVA followed by Tukey's multiple comparisons tests (**o**). **r** si-LXRβ upregulated the level of IL-1β and TNF-α in hippocampal tissue under 24-HC. $n = 4$ mice in each group. Data were normalized to the mean value of control group. Data are presented as mean ± SD. Two-way ANOVA followed by Tukey's multiple comparisons tests. **s** A cartoon illustrating the pathway for 24-HC to target on LXRβ, and facilitate its transcriptive suppression on pro-inflammatory factors. Source data are provided as a Source Data file. Certain illustrative components in panels (**k** and **s**) are created in BioRender. Zheng, J. (2026) https://BioRender.com/c9dsmfb.

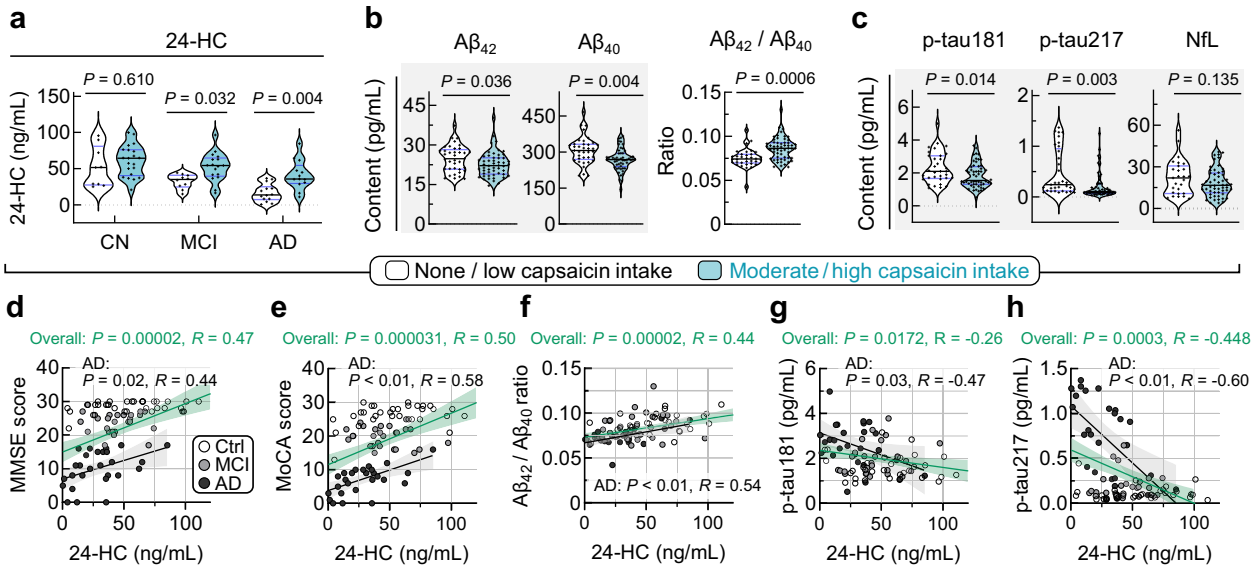

Fig. 8 | Moderate-to-high capsaicin intake associated with elevation of 24-HC and lower levels of plasma pathologic biomarkers in AD patients. a MCI and AD subjects with moderate-to-high capsaicin intake from chili-rich diets has higher levels of 24-HC in the plasma. $n = 95$ in total, Data are presented as median with quartiles. two-way ANOVA followed by Tukey's multiple comparisons tests. **b**, **c** Human subjects with moderate-to-high capsaicin intake had lower levels of $A\beta_{42}$ and $A\beta_{40}$, but higher $A_{\beta 42}$ / $A\beta_{40}$ ratio (**b**), as well as lower levels of plasma p-tau181 and p-tau217. Limited change in NfL was found (**c**). Unpaired *t* tests. Data are presented as median with quartiles. The level of plasma 24-HC positively correlated with MMSE score (**d**), MoCA score (**e**), and Aβ42 / Aβ40 ratio (**f**), while negatively correlated with plasma p-tau181 (**g**) and p-tau217 (**h**). Those associations were significant both in overall cohort 2 (green lines) and in the AD subset (gray lines). Simple liner regression analysis. Light green and gray bands indicate 95% confidence interval of indicated groups. Source data are provided as a Source Data file.

capsaicin were observed in both 5×FAD mice, P301S mice and AD patients.

In consistent with our findings, a cross-sectional study in human also found that capsaicin diet consumption positively correlated with cognitive improvement and negatively correlated with serum Aβ lvel[53]. Similarly, in APP/PS1 mice, capsaicin treatment in food reduced both Aβ burden and rescued cognitive decline[54]. Nevertheless, the exact effect of capsaicin on cognitive function is still controversial to date[5]. A follow-up study over 15 years revealed that people with chili consumption over 50 g per day had globally lower cognitive score than chili non-consumers[55]. The discrepancy might stem from the difference in chili consumption dosage, tolerance or preference, and measurement criteria across cohorts. In fact, different doses of capsaicin might induce different outcomes. For example, low doses of capsaicin (≤5 mg/kg) have found to enhance beneficial bacteria like *Firmicutes, Lachnospiraceae*, and *Blautia*, which increased butyrate production and improve gut barrier function. Moderate doses of capsaicin further boosted probiotics such as *Akkermansia* and *Faecalibacterium prausnitzii*, thus enhancing insulin sensitivity and anti-inflammatory activity. However, high doses of capsaicin (>10 mg/kg) disrupted microbial balance by increasing *Bacteroidetes* while depleting mucin-degrading bacteria (*Akkermansia, Lachnospiraceae*), which may impair intestinal integrity, elevate permeability, promote bacterial translocation, and create a pro-inflammatory/metastatic environment[56–58]. These findings suggest a shift of capsaicin's effects from beneficial at low-to-moderate doses to detrimental at supraphysiological high doses. Here, we only included subjects of chili consumption within the physiological range in human studies, and measured the effect of capsaicin ranging from

0.01 to 1 mg/kg in mice. It is to be elucidated in the future whether repeated administration of capsaicin at much higher dosages will produce more beneficial effects, or turn to exacerbate the pathogenesis of AD.

Capsaicin in diets is passively absorbed in the stomach and guts after oral intake, distributes to blood and organs, and can be completely metabolized within approximately four days[59,60]. Although it has been reported that direct intraperitoneal injection of capsaicin in mice were effective in alleviating cognitive and synaptic impairments in AD mouse models, it remains indefinite whether capsaicin in periphery can cross the blood-brain barrier to directly act on neurons or glia in the brain. In the present study, we found that after repeated oral administration, capsaicin was most abundant in the stomach and intestinal contents, followed by intestinal tissue, stomach tissue, and liver tissue. However, only minimal levels were detected in the brain, suggesting very limited absorption of capsaicin into the brain. Here, we initially hypothesized that the beneficial effects of oral capsaicin treatment on AD is mediated by the well-known capsaicin receptor TRPV1, expressing either on peripheral/central neuronal fibers or non-neuronal cells in peripheral organs[61]. Unexpectedly, it was found that capsaicin intake still effectively ameliorated AD phenotypes in TRPV1 global knockout mice. Thus, we shifted our focus to the intestinal tract contents, where capsaicin was found to be most abundant.

Oral administration of capsaicin induced significant gut microbiota remodeling in AD mice, characterized by increased *Firmicutes* enrichment and reduced abundance of *Bacteroidetes*, *Proteobacteria*, and *Verrucomicrobia* at the phylum level. These findings align with previous reports of capsaicin's modulatory effects on gut microflora in diabetic and high-fat diet-induced obese mouse models[62–65]. Accumulating evidence suggests a critical role of gut microbiota in the pathogenesis of AD. Both MCI and AD patients exhibit characteristic gut microbial alterations, including decreased *Firmicutes* and increased *Proteobacteria* abundance[66]. Direct supplement of probiotic like *Faecalibacterium prausnitzii, Lactobacillus casei* and *Lactobacillus acidophilus* belonging to the *Firmicutes* phylum showed therapeutic potentials in preclinical studies[67,68]. Here, we found that capsaicin intake specifically increased the abundance of such as *Oscillospiraceae* and *Clostridiaceae* family, and ascertained the capacity of Oscillibacter genus belonging to the *Oscillospiraceae* in producing 24-HC. It deserves further investigation whether and how other gut bacteria like *Alistipes* genus contribute to the capsaicin's beneficial effects against AD. Of note, while our findings indicate that gut microbiota remodeling represents a key downstream response to oral capsaicin treatment, potential extra-intestinal effects may still exist. For example, persist activation of TRPV1 by capsaicin in the autonomic nervous system could potentially modulate host's voluntary preferences for capsaicin-rich foods, affect the absorption of capsaicin, or regulate non-inflammatory responses in the brain.

Intriguingly, while pan-depletion of gut microbiota by ABX alleviated AD-associated pathologies[31,32], we found ABX abolished the anti-AD effects of capsaicin. A possible explanation is that ABX alone prevented gut dysbiosis and reduction of harmful metabolites, while also inevitably leads to the depletion of gut probiotics, thereby eliminating the basis of gut microbiota-dependent therapeutics. Consequently, while ABX treatment may globally attenuate AD pathological phenotypes, it simultaneously abolishes capsaicin's beneficial effect like the modulation of 24-HC metabolism through microbiota-dependent mechanisms.

Regulation on host metabolism is the pivotal way for gut microbes to bridge diet with the gut-brain axis. Our findings demonstrate that oral capsaicin administration primarily alters 24-HC metabolism in a gut microbiota-dependent manner. The levels of 24-HC in intestinal contents, blood and brain of either WT or 5xFAD mice were all reduced by global depletion of gut microbiota by co-utilization of ABX with capsaicin. By contrast, specifically suppression of local 24-HC production in the brain by inhibiting CYP46A1 did not change 24-HC in the gut, but only reduced 24-HC in the brain and blood, the latter might be attributed to capacity of 24-HC in the brain to penetrate BBB and enter into the blood[69,70]. Indeed, a group of microbial enzymes encoded by ismA genes has been found to dehydrogenate cholesterol in gut[20]. Bacterial species from the *Oscillibacter* genus in *Firmicutes* phylum were significantly associated with the decreased cholesterol levels in fecal and plasma[17]. Additionally, *Bacteroides* were found to contribute to cholesterol metabolism through the sulfotransferase BT0416[18,19]. In consistent with our results here, randomized controlled trials also showed that capsaicin consumption was negatively correlated with both total cholesterol and low-density lipoprotein cholesterol levels in the blood of patients with metabolic syndrome[71], and mice treated with capsaicin had changes in the relative abundance of short-chain fatty acids-producing gut microbes[72,73], which might be also involved in the metabolism of cholesterol and 24-HC. Nonetheless, specific bacterial gene sets and enzymes that responded to the oral administration of capsaicin and regulate 24-HC production remained to be elucidated in the future.

Elevation of 24-HC in the plasma and brain was found here to protect against AD both in 5×FAD and P301S mice. Consistently, upregulation of 24-HC synthesis in the brain through genetic overexpression of CYP46A1, which converts cholesterol to 24-hydroxycholesterol specifically in the host central nervous system, was found effective to improve memory and inversely correlated with neurodegeneration biomarkers in females[33]. Pharmacological activation of CYP46A1 using efavirenz in 5×FAD mice of both sexes showed effectiveness in reducing Aβ plaques and improving cognitive function[34,74]. Besides, direct supplement of 24-HC also prevented Aβ-induced hyperphosphorylation of tau in transgenic mice expressing human tau, possibly through enhancing the neuroprotective effect deacetylase sirtuin-1[75]. Nevertheless, both the change of 24-HC in the brain of AD patients and its contribution to the pathogenesis of AD were still controversial[76]. 24-HC treatment at 50 μM for 16 h in cultured macrophages increased the TNF-α level[77]. Lowering 24-HC in the brain of APP/PS1 mice using soticlestat reduced premature deaths of mice presumedly through suppressing neuronal hyperactivation[42], while how it affects AD development in adult mice are to be examined. Additionally, it is intriguing that, despite of high similarity in structure, 24-HC, 25-HC, and potentially other hydroxycholesterols may exert divergent regulatory effects on neuroinflammation and AD-related phenotypes. For instance, 25-HC has been found to promoted proinflammatory cytokines production and impair microglial phagocytic capacity[78–80]. These effects might collectively exacerbate neuroinflammation and amyloid pathology in AD.

In contrast, the effects of 24-HC on neuroinflammation and AD appear to be more complex[81]. 24-HC treatment at 50 μM for 16 h in cultured macrophages increased the TNF-α level[77], while upregulation of local 24-HC in the brain of 5xFAD mice via CYP46A1 overexpression was found to ameliorate neuroinflammation, amyloidosis and improved cognition functions[82]. Similar protective effects of 24-HC were also widely observed under treatment of efavirenz, a positive allosteric modulator of CYP46A1[34,74,83]. Moreover, 24-HC prevented tau hyperphosphorylation induced by Aβ monomers in h-tau transgenic mice[75], and cerebrospinal fluid levels of 24-HC was found to negatively correlate with neurodegeneration markers in a clinical cohort of AD patients[33]. The complexity of 24-HC actions may be attributed to factors such as its concentration-dependent effects and the duration of exposure. Collectively, these findings present compelling evidence for an intriguing dichotomy that, despite of high similarity in structure, 24-HC, 25-HC, and potentially other hydroxycholesterols may exert divergent regulatory effects on neuroinflammation and AD-related phenotypes. The underlying mechanisms responsible for these functional differences deserve in-depth investigation in future studies.

We found direct supplement of 24-HC or oral administration of capsaicin in AD mice alleviated microglia malfunction through facilitating the effect of LXRβ on suppressing the gene expression of inflammatory factors. In fact, the anti-inflammatory effect of LXRβ has been widely recognized in macrophages[45]. Activating LXRβ using its another agonist GW3965 can also promote microglia phagocytic activity and attenuate inflammatory response to fibrillar Aβ, while genetic knock-out of LXRβ in APP/PS1 mice significantly increased the Aβ burden[84]. Notably, ligand-bound LXRβ can be SUMOylated to promote its localization to NF-κB or other responsive elements to form transcriptive corepressor complex, thereby to inhibit gene expression of pro-inflammatory factors such as IL-1β, IL-6, TNF-α and inducible nitric oxide synthase (iNOS)[85,86]. As a result, higher portion of microglia would switch from the proinflammatory subtype to the anti-inflammatory type, which is beneficial for the phagocytosis of extracellular Aβ[87].

Besides, since excessive activation of microglia and inflammation were also involved in the AD-related tau pathology, suppression of microglia dysfunction has been found effective to downregulate tau hyperphosphorylation and spreading[48]. Therefore, we observed here in different mice model that capsaicin or 24-HC not only ameliorated Aβ burden but alleviated tau pathology, and the level of 24-HC significantly correlated with both p-tau and Aβ markers in the plasma of AD patients. Direct evidence of how the gut microbiota changes in P301S mice at 5 – 6 months of age and how it correlates with tau-related pathology remains unclear to date. In TE4 mouse line expressing human tau-P301S and ApoE4, it was noted that, at 12 weeks of age, TE4 mice reared in a germ-free environment for less invasively depleting gut microbiota also tended to exhibit reduced microglial activation[88]. In another study using ADLP^{APT} mice, a line exhibiting both Aβ and tau pathologies in the brain, researchers observed significant alterations in gut microbiota composition as early as 2 months of age, while transplanting gut microbiota from healthy mice starting at this early stage for a duration of 4 months effectively reduced both Aβ- and tau-related pathological phenotypes and cognitive deficits[15].

Notably, 24-HC has been also shown to exert dual effects on neural cells. In neurons, 24-HC functioned as a positive allosteric modulator of NMDA receptors and activated estrogen receptors-mediated sex hormone signaling, both of which potentiated synaptic plasticity and memory in mice[33,89,90]. Additionally, 24-HC induced proteolysis of tau through the activating the SIRT1/PGC1α/Nrf2 axis[91]. In astrocytes, 24-HC promoted cholesterol transport via ApoE and LXR-mediated pathways[92]. However, the roles of 24-HC in AD remains complex and context-dependent. While physiological levels appear neuroprotective, elevated concentrations (25–50 μM) have been reported to induce oxidative stress, amplify Aβ toxicity in neurons[93], and trigger astrocyte reactivity[74]. This dose-dependent dichotomy warrants further systematic investigation.

In addition, we focused here the protective effects against AD of capsaicin-induced upregulation of 24-HC levels, while potential roles of other metabolites also exist. Especially, significant reduction of plasma cholesterol was also observed following capsaicin treatment. Multiple cohort studies have revealed a significant correlation of blood low-density lipoprotein cholesterol (LDL-C) level with the risk of AD and dementia[94,95], as well as cerebral amyloidosis imaging index[96]. Excessive uptake of peripheral cholesterol drives a major component of chronic inflammation in the brain through dysregulating glia activation, and promotes Aβ secretion and tau hyperphosphorylation[21,97]. Consistently, reduction of cholesterol level is effective for alleviating neuroinflammation and AD pathologies[22,98]. These findings raise the possibility that capsaicin could also mediate its protective function through the downregulation of cholesterol levels. Besides, our metabolomic data also suggest an alteration of plasma bile acid following the capsaicin treatment, which has been found to be associated with the development of AD[99,100]. Elucidating these alternative pathways is of significant scientific interest.

There are several other limitations in the present study. We used only male mice in animal experiments, the potential sexually dimorphic response and underlying mechanisms warrant further investigation, especially given the definite correlation between lipid metabolism and estrogen signaling, and a previous study has reported that the cognitive-enhancing effects of local 24-HC overproduction in the brain is only pronounced in ovariectomized female mice, but not in gonadectomized male mice[33]. Besides, other mechanisms underlying the beneficial effects of 24-HC are also to be elucidated. Intriguingly, in addition to its anti-inflammatory function, LXRβ also play as a sensor or regulator of cholesterol absorption, transport, efflux, excretion and conversion[101]. It is unclear whether and how the host regulation of cholesterol metabolism through LXRβ contributes to be capsaicin-induced anti-AD effects, especially at stages following the initial elevation of 24-HC mediated by gut microbes. Besides, the effect of capsaicin-rich diets on the onset or development of AD is to be investigated and followed-up in larger cohorts in the future.

To summarize, we found here that dietary intake of capsaicin promoted gut microbiota-dependent anabolism of 24-HC, which enhance the LXRβ-mediated suppression of microglia activation and inflammation in the brain, thereby contributing to the amelioration of AD-related Aβ and tau pathologies in the brain. These results suggest the potential of capsaicin or analogs in the prevention or treatment of AD and related diseases.

Methods

Ethical approval

All studies in human were conducted under the informed consent from participants, and were approved by the Medical Ethics Committee of the Affiliated Hospital of Zunyi Medical University (KLL-2020-074), or the Medical Ethics Committee of Peking University Sixth Hospital (2023LS#38). All animal experiments in this study were approved by Medical Ethics Committee of the Affiliated Hospital of Zunyi Medical University (KLL-2020-075), and the Animal Care and Use Committee of Peking University (LA2022088).

Human cohorts

This study was conducted under the informed consent from participants. Cohort 1 were recruited from the retirement community in Huichuan District, Zunyi, China, and cohort 2 were recruited form the Department of Neurology, Peking University Sixth Hospital, Beijing, China. Excluding criteria included: (1) Age <40, (2) having history of neurological disorders that potentially leading to cognitive impairments, like stroke, brain tumor, brain trauma, brain infection, etc., (3) having foreign objects like peacemaker in body, (4) having psychological disorders like bipolar disorders, major depression, etc., (5) having history of drug abuse, (6) currently having common cold or allergic rhinitis, (7) having anosmia, severe hearing and visual impairment, (8) illiterate, (9) not suitable to participate in this study for other reasons. Finally, a total of 151 subjects in cohort 1 and 95 subjects in cohort 2 were included.

All subjects in the cognitively normal (CN) group did not report any memory complaints or subjective cognitive decline during interviews. Moreover, CN subjects were further identified based on the criteria: (1) MMSE score ≥ 27 and/or MoCA score ≥26, (2) absence of AD-like pathology as confirmed by clinic diagnosis supported by results from MRI imaging and/or cerebrospinal fluid or plasma biomarkers (e.g. p-tau217, Aβ42). MCI or AD individuals meet the diagnostic criteria for MCI and AD established by the National Institute on Aging and the Alzheimer's Association (NIA-AA) 2018[102]. Diagnosis was performed by experienced experts in clinic.

Only participants of comparable age, gender and education levels were included for analysis. Information of capsaicin intake and

cognitive function were measured using a specific diet questionnaire (Supplementary Data 2), MMSE and MoCA, respectively, at a specific meeting room in community for cohort 1 or consulting room in Peking University Sixth Hospital for cohort 2. For each subject in the cohort 2, plasma was separated within 3 h following blood sampling and then stored under −80 °C.

Animals

Wildtype C57BL/6 J mice were provided by the Department of Laboratory Animal Sciences, Peking University Health Science Center (Beijing, China). 5×FAD mice (B6.Cg-Tg(APPSwFlLon,PSEN1*M146L*L286V)6799Vas/Mmjax), Trpv1 KO mice (B6.129×1-Trpv1tm1Jul/J), P301S mice (B6;C3-Tg(Prnp-MAPT*P301S)PS19Vle/J) and Cx3cr1-CreERT2 (B6.129P2(Cg)-Cx3cr1tm2.1(cre/ERT2)Litt/WganJ) were purchased from Shulaibao Biotech Co., Ltd (Wuhan, China) or Jackson Laboratory. Adult male mice were used in experiments. All transgenic mice for mimicking AD-associated pathologies were breed from paternal origin[103]. To control for potential transfer effects of gut microbiota, transgenic mice and WT littermates were kept separately in different cages throughout experiments. All mice were provided with ad libitum access to food and water, and kept under the specific-pathogen-free (SPF) conditions at 22 °C, with 50–60% humidity, 12 h/12 h light/dark cycle. SPF laboratory rodent diets compliant with the AIN-93G and AIN-93M standards purchased from Beijing Beiluo Biotechnology (XT-SPF-2) was used.

Reagents and resources

Key resources used in this study including antibodies, critical chemicals, commercial assays, animals and cell lines, deposited data, software were summarized in the Supplementary Data 7. All antibodies are commercially available and have been validated by the manufacturers, as well as validated presently by different experimenters in our team or previously by different labs in our institute.

Drug treatment in mice (capsaicin, LPS, SOT, 24-HC)

In the present study, drug treatments in AD models and age-match WT controls (capsaicin, ABX, 24-HC, SOT) begun at 5-month of age, while treatments solely in WT mice (capsaicin, LPS) begun at 3-month of age. Capsaicin was dissolved in 1% ethanol and administrated intragastrically (i.g.) once per day for consecutively 30 – 40 days, at each dose of 0.01 – 1 mg/kg of mouse body weight for normal WT mice, or 1 mg/kg for 5×FAD, LPS-treated WT and P301S mice. Equal doses of 1% ethanol were orally gavaged as control. Lipopolysaccharide (LPS) was intraperitoneally (i.p.) injected in WT mice at 0.25 mg/kg for mice body weight once every other day for a month to induce neuroinflammation in the brain[27]. Equal amount of normal saline (NS) was injected as control. SOT was co-administrated with 24-HC via oral gavage in 5×FAD mice for 40 days at the dose of 50 mg/kg of body weight once per day[42], and NS was used as control. 24(S)-hydroxycholesterol (24-HC) was intraperitoneally injected in 5×FAD mice at 0.01 mg/kg (dissolved in DMSO, 0.15 mL in volume) of body weight in 5×FAD mice every two days for a consecutive month. An equal amount of DMSO solution was injected in control.

Animal behavior tests

Object-place recognition and novel-object recognition tests. Mice were handled for 5 min per day for 3 consecutive days before the first behavioral test. In the probe phase, mice were placed in a chamber of 50 × 50 × 50 cm which was marked with visual cues on the wall, and two identical plastic toys (termed object A and B) were placed at the two different corners. Each mouse was placed into the chamber and allowed to freely explore for 5 min, then removed from the box and stayed in the home cage for 30 min, during which the chamber and the objects were cleaned with 75% ethanol. In a pseudorandom way, one of the two objects (object B) was moved to a new corner while the other object (object A) remained unmoved. In the test phase, each mouse was placed back into the chamber and allowed to freely explore for another 5 min. Mouse behaviors were recorded by digital camera, and videos were analyzed offline using an ANY-maze video tracking system (Stoelting, USA). The time mice spent within the area around each object (radius = 5 cm) was counted as exploring and the preference ratio towards object B was calculated as the exploring time (B − A) / (B + A)[104].

Novel-object recognition tests were performed at the next day following the object-place recognition test. A similar protocol was used except that the object B was replaced by a novel object (object C) in the test phase, and mice preference to the novel object was measured as the exploring time (C − A) / (C + A).

Morris-water maze test. In the learning phase, mice were trained to find a hidden platform submerged under water in a water maze of 1.2 m in diameter for three trials per day and consecutive of 6 days. Four visual cues outside the pool remained constant. In each trial, in a pseudorandom way, mice were placed in one of the three quadrants without platform and allowed to freely seeking. If failed to find the target within 60 s, the mouse would be guided using a wooden stick to find the platform and allowed to stay here for another 10 s. At the test day, each mouse was placed in the water maze with the hidden platform removed, and allowed to freely swim for 60 s. The traveling path of each mouse was recorded by a digital camera, and videos were analyzed offline using an ANY-maze video tracking system (Stoelting, USA).

Fear conditioning. Fear conditioning test were performed at the last of series behavioral tests. Each mouse was placed in a conditioning chamber of 23 × 23 × 30 cm, with the floor made of steel rods wired to a shock generator. At day 1, each mouse was placed in the chamber and allowed to explore for 3 min. A 2-s foot-shock of 65 mA was then delivered, and then the mouse was allowed to stay in the chamber for another 1 min. The chamber was cleaned with 75% ethanol between each animal. At the next day, mice were placed back in the chamber and allowed to freely explore for 3 min, but no foot-shock was delivered. Freezing behavior of mice were measured online using an FCT-100 system (Techman, China).

Open field test. Each mouse was placed in a chamber 60 × 60 × 60 cm without top cap, allowed to travel freely for 5 min under the context of 60 lux illumination. Mice behaviors were recorded by a digital camera, and the time of mice spent in the central area of chamber (30 × 30 cm) and total distance traveled in the chamber were analyzed offline using an ANY-maze video tracking system (Stoelting, USA). The box was cleaned by 75% ethanol between tests.

Elevated plus-maze test. The maze was consisted of two open arms and two closed arms (5 × 30 cm and 15 cm wall height for the closed arms), placing 50 cm above the floor in a 5-lux illuminated room. Each mouse was placed onto the crossing center of maze, heading toward a same open arm, and allowed to freely explore for 5 min. Mice behaviors were recorded by a digital camera, and the time of mice spent in the open arms were analyzed offline using an ANY-maze video tracking system (Stoelting, USA). The maze was cleaned by 75% ethanol between tests.

ELISA

ELISA kits for the detection of human Aβ 1-40 and Aβ 1-42, mouse IL-1β and TNF-α were purchased from Elabscience (Supplementary Data 7). All procedures followed the manufacturer's instructions, signals were measured at 450 nm in a Varioskan LUX Multimode Microplate Reader (Thermo Fisher). In brief, mice were executed by cervical dislocation. Dorsal part of hippocampal tissue was isolated on ice, homogenized

with RIPA lysis buffer (HY-K1001, Beyotime), and then centrifuged at 4 °C, 11,300× *g* for 30 min. The supernatants were collected for the detection of soluble Aβ, inflammatory factors or capsaicin, and the pellets were resuspended with 70% formic acid for the measurement of insoluble Aβ.

For the measurement of capsaicin, samples prepared from mice stomach and small intestinal contents, or tissues of stomach, small intestinal, liver and hippocampus formation were isolated, respectively, homogenized using distilled water, and centrifuged at 2500 × *g* for 10 min, the supernatant was collected for analysis using a High Sensitivity Capsaicin ELISA Kit purchased from Creative Diagnostics (NY, USA) (Supplementary Data 7) based on the principle of competitive binding of capsaicin to the antibody of the capsaicin-enzyme conjugate. All procedures followed the manufacturer's instructions, signals were measured at 450 nm in a spectrophotometer (Thermo Fisher).

Brain section preparation

Mice were anesthetized with 1% pentobarbital sodium and intracardially perfused in turn with saline and 4% paraformaldehyde (in 0.1 M phosphate buffer, pH 7.4). Mice brains were removed, post-fixed in 4% PFA for 12 h, and then cryoprotected in 20 – 30% sucrose solutions. Brain sections of 35 mm thickness were sliced in a cryostat microtome (FS800, RWD Life Science).

Immunofluorescent staining

Free-floating brain sections washed in PBS, blocked in a buffer containing 5% bull serum albumin and 0.3% triton x-100 for 1 h, and then incubated with primary antibodies (1:200 ~ 1:500 dilution in 0.3% PBST) at 4 °C for 24 h. After washed in PBS, sections were incubated with HRP-conjugated goat anti-mouse IgG (1:500 dilution in 0.3% PBST for all antibodies) and DAPI (1:10,000) at 37 °C for 1.5 h, and finally mounted with a buffer containing $NaHCO_3$ (220.2 mM), Na_2CO_3 (28.3 mM) and 50% glycerol. Antibodies used in this study were summarized in the Supplementary Data 7. Images were taken by a laser-scanning confocal microscope (LSM880, Zeiss).

Aβ plaques staining and analysis

For immunohistochemistry staining of Aβ plaques by 6E10, free-floating brain sections were incubated with PBS containing 0.3% H_2O_2 and 0.5% triton x-100 in for 15 – 30 min at room temperature, washed with PBST, and then treat with 70% formic acid for 30 min. Subsequently, after washing with PBST for 4 × 5 min, brain sections were blocked using 5% bull serum albumin (BSA), incubated with 6E10 antibody at 4 °C for 24 h (1:200 dilution in 0.3% PBST). After washed in PBS, sections were incubated with HRP-conjugated goat anti-mouse IgG at 37 °C for 1.5 h (1:500 dilution in 0.3% PBST for all antibodies). Immunoreactions were developed using a DAB-staining kit (ZLI9018, ZSGB-BIO). Sections were then dehydrated through graded ethanol series, with or without counterstaining with a Nissl staining solution (Beyotime), and finally sealed with neutral balsam. Images were taken by a digital slide scanner (Pannoramic SCAN II, 3DHISTECH), and analyzed using the Fiji software[105].

For immunofluorescent staining of Aβ and Iba1, experimental procedures were in similar with the immunohistochemistry staining except for the additional 0.3% H_2O_2 incubation before the BSA blockage. Images were taken by a laser-scanning confocal microscope (LSM880, Zeiss), and analyzed using the Imaris v10.1 software (Oxford Instrument).

Microglia morphology analysis

For the analysis of microglia morphology, z-stack fluorescence images of Iba-1 immunostaining were acquired by scanning throughout sections of 35 μm thickness at 3 μm intervals, and then imported into the Imaris software (v10.1, Oxford Instruments). Only cells located in the stratum radiatum layer of hippocampal CA1 were selected for analysis. 3D morphology of cell processes was reconstructed using the *Filament* module, and processes complexity were measured using Sholl analysis. Cell soma were reconstructed using the *Surface* module, and soma volume were measured. About 8 – 10 cells in each section, and a total of 3 sections at similar coronal levels were analyzed for each mouse. The results of all cells from each mouse were averaged.

Western blotting and co-immunoprecipitation

Hippocampus tissues or cultured cells were collected on ice, then homogenized and cytoplasmic and nuclear proteins were separated using a Nuclear Protein Extraction Kit (EX1470, Solaribo) containing protease and protein phosphatases inhibitors cocktail in accordance with the manufacture's instruction. Protein concentration was measured through BCA assays (23225, Thermo Scientific). Equal amount of protein from each sample were separated in SDS-PAGE gels, and then transferred onto nitrocellulose membranes (Merck Millipore). The membranes were blocked with 5% BSA, and incubated in turn with primary and horseradish peroxidase-conjugated secondary antibodies. All antibodies used in this study were summarized in the Supplementary Data 7. Blots were visualized using the ECL luminol reagent (P0018S, Beyotime), and quantified using ImageJ software.

For co-immunoprecipitation, cultured cells or hippocampus tissue were lysed. Nuclear proteins were separated, incubated with protein G agarose at 4 °C for 2 h, and then centrifuged for 5 min (4 °C, 11,000 × *g*). Supernatants were then incubated with specified mix of primary antibodies and protein G agarose overnight at 4 °C. The agarose beads were collected through centrifugation at 4 °C, 11,000 × *g*, and then washed three times with PBS, and resuspended in a loading buffer containing 2% SDS, 100 mM dithiothreitol, 10% glycerol, and 0.25% bromophenol blue. The mixture was denatured at 95 °C for 5 min. Immunoprecipitants were then detected through Western blotting.

Bulk RNA sequencing

Mice were executed by cervical dislocation. Brains were acutely removed and hippocampus formation were isolated on ice, grinded in liquid nitrogen. Samples were dissociated and total RNA were isolated using the TRIzol reagent (Life technologies, USA). Bulk RNA sequencing was performed by BMKGENE (Beijing, China). In brief, concentration and integrity of RNA sample were examined by NanoDrop 2000 (Thermo Fisher) and RNA Nano 6000 Assay Kit of the Agilent Bioanalyzer 2100 system (Agilent Technologies, USA), respectively. Sequencing libraries were generated using Hieff NGS Ultima Dual-mode mRNA Library Prep Kit for Illumina (Yeasen Biotechnology (Shanghai) Co., Ltd.) following manufacturer's recommendations and index codes were added to attribute sequences to each sample. RNA sequencing was conducted on the Illumina NovaSeq platform with paired-end 150-bp reads. Clean reads of each sample were mapped to specified reference genome and quantified using HISAT2 and StringTie. Differentially expressed genes (DEGs) were identified using the criteria of Fold Change≥1.5 and FDR < 0.05. GO enrichment analysis was performed through the clusterProfiler package. RNA sequencing data associated with this project have been deposited in the NCBI-SRA database (https://www.ncbi.nlm.nih.gov/sra, accession number: PRJNA1173896).

RT-qPCR

Mice hippocampus tissue or cultured bacteria were collected on ice, and subsequently snap-frozen in liquid nitrogen. Total RNA was extracted utilizing TRIzol reagent (15596018, ThermoFisher). RNA purity and concentration were assessed via a NanoDrop spectrophotometer, and cDNA synthesis was performed with 1 μg of total RNA using the PrimeScript RT Reagent Kit (RR037B, Takara Bio), incorporating genomic DNA eraser to prevent genomic DNA contamination. qPCR reactions were

executed in triplicate using Taq Pro Universal SYBR qPCR Master Mix (Q712-02, Vazyme) on a Bio-Rad CFX96 Real-Time PCR System. Each 20 μL reaction comprised 10 μL SYBR Green mix and 0.4 μM of each forward and reverse primers (Supplementary Data 8) synthesized by Tsingke (Beijing, China), β-actin or universal bacterial 16S rRNA was used as internal controls. Assays with amplification efficiencies between 90% and 110% and a single peak in melt curve analysis were considered valid, otherwise, the RNA level was set to 0.

Metagenome sequencing

Mice were executed by cervical dislocation. Contents of the entire small intestines were collected, homogenized using PBS, and then centrifuged at 11,000 × *g* for 10 min. The supernatant was used for total genomic DNA extraction utilizing a PowerSoil® DNA Isolation kit (#200059-790, Mo Bio Laboratories, USA) according to manufacturer's instructions. The quality and quantity of DNA were examined using Qubit dsDNA HS Assay Kit on a Qubit 3.0 Fluorometer (Life Technologies, USA) and electrophoresis on a 1% agarose gel, respectively. Metagenome sequencing was performed by BMKGENE (Beijing, China). Briefly, paired-end libraries (insert size, ~350 bp) were prepared using a VAHTS Universal Plus DNA Library Prep Kit for Illumina (ND627-01, Vazyme Biotech). The library was sequenced on Illumina NovaSeq 6000 platform using the 150-bp paired-end sequencing mode. The two paired FASTQ files were base called from the Illumina raw sequence read data. The quality of the raw sequence reads was assessed using Trimmomatic (v0.33)[106]. After trimming the adaptors and filtering low-quality reads, the clean sequence data were used for further bioinformatics analysis. Reads were aligned to the mouse genome by bowtie2 (version 2.2.4) and any hit associated with the reads and their mated reads were removed[107]. Metagenomics data were assembled using MEGAHIT[108]. Assembly summary statistics were determined using QUAST software v2.3[109]. Contigs with the length being or over 300 bp were selected as the final assembling result, and then the contigs were used for further gene prediction and annotation. Open reading frames from each assembled contig were predicted using MetaGeneMark (http://exon.gatech.edu/meta_gmhmmp.cgi). All predicted genes with a 95 % sequence identity (90% coverage) were clustered using MMseqs2 (https://github.com/soedinglab/mmseqs2). Representative sequences of non-redundant gene catalog were aligned to NCBI NR database with e-value cutoff of 1e-5 using Diamond software for taxonomic annotations. GO annotation was performed by Blast2GO (v2.5.0) with Pfam annotations. The KEGG annotation was conducted using Diamond (v0.9.29) against the Kyoto Encyclopedia of Genes and Genomes database (http://www.genome.jp/keeg/) with an e-value cutoff of 1e-5. Metagenome sequencing data associated with this project have been deposited in the NCBI-SRA database (https://www.ncbi.nlm.nih.gov/sra, accession number: PRJNA1173905).

Gut microbiota transfer (GMT)

Capsaicin (1 mg/kg per day) or equal dose of vehicle was orally administrated to 5-month 5xFAD, respectively, for a month. Gut contents were aseptically collected and immediately transferred to an anaerobic chamber (85% N_2, 10% H_2, 5% CO_2). Contents from both the small intestine and colon were included here, since colon have been recognized to have higher abundance of microbes. The contents were homogenized in pre-reduced PBS and centrifuged at 11,000 × *g* for 10 min at room temperature. The pellets were washed three times with PBS under the same centrifugal conditions (final solvent at 1 mL per gram of gut contents). To remove residual capsaicin, the final supernatant was mixed with pre-reduced sterile corn oil, vortexed for 2 min, and allowed to phase-separate for 10 min. The lower aqueous layer containing gut microbes was carefully recovered, sealed and preserved at −80 °C in PBS with 40% glycerol and 0.001% L-cysteine. Frozen samples were thawed at 4 °C for 12 h prior to use and subsequently administered to 5-month 5xFAD mice via oral gavage (0.5 mL each day, once every other day for a month). Equal doses of PBS were delivered as negative control.

ABX treatment

ABX was orally gavaged as previously descibed[10]. In brief, an aliquot of 0.2 mL antibiotic cocktail (1 mg/mL ampicillin, 0.5 mg/mL vancomycin, 1 mg/mL metronidazole, 1 mg/mL neomycin and 0.01 mg/mL amphotericin B) was administrated once every day for each mouse, beginning at 5-month of age and 7 days before the capsaicin administration and maintained throughout the entire experiment. To validate the effect of ABX on depleting gut microbes, the contents of small intestine were collected after mice execution, and then homogenized using PBS. Samples were subsequently centrifuged at 800 × *g* for 10 min. The supernatant was either cultured on Luria-Bertani agar plate for 24 h under normal conditions and colonies formation of aerobic bacteria was examined, or cultured in Gifu anaerobic medium under oxygen-free environment for 24 h and the optical density (O.D.) of bacterial fluid was measure at 600 nm.

Untargeted metabolite profiling

Blood samples were acquired from male vehicle- or capsaicin-treated WT C57BL/6 and 5xFAD mice (6 months of age, $N = 15$ mice in total and 5 mice per group), centrifuged at 4 °C, 800 × *g* to separate the plasma and then stored under −80 °C until experimental analysis. Untargeted metabolome analysis was performed by BMKGENE (Beijing, China). In brief, an aliquot of 100 μL from each sample was mixed with a buffer of methanol / acetonitrile = 1:1, v/v containing internal standard (L-2-chlorophenyl alanine), ultrasonicated for 10 min on ice, and then placed under −20 °C for one hour. Samples were subsequently centrifuged at 4 °C, 11,000 × *g* for 15 min. About 500 μL supernatant was dried in vacuum concentrator, and then reconstituted with 160 μL 50% acetonitrile (in ddH_2O) on ice, centrifuged again at 4 °C, 11,000 × *g* for 15 min. The supernatant was collected, and analyzed using a ACQUITY UPLC I-Class PLUS System combined with Xevo G2-XS QTof (Waters, USA) under either positive and negative modes, respectively. Columns of 1.8 μm 2.1 * 100 mm (Acquity UPLC HSS T3, Waters, USA) were used. The mobile phase was 0.1% formic acid diluted in ddH_2O and acetonitrile, and 1 μL of samples was injected. Raw data acquired in the MassLynx software (v4.2) was processed using Progenesis QI software (Waters, USA), and metabolites were identified by METLIN. The deviation of mass is controlled within 100 ppm. Metabolome data associated with this project have been deposited in the Supplementary Data 5. KEGG annotation was conducted using Metaboanalyst (https://www.metaboanalyst.ca/), and the correlation analysis among microbe genus abundance, metabolites level, and relative functional gene abundance were performed using the igraph, ggalluvial and Hmisc packages.

LC-MS/MS measurement of 24-HC

Mice or human blood were collected and then centrifuged to separate the plasma. Hippocampus tissue or small intestinal contents of mice were isolated on ice, then homogenized with PBS containing 5 mM EDTA and 50 μg/mL butylated hydroxytoluene (pH 7.4), centrifuged at 4 °C, 11,300 × *g* for 10 min, the supernatants were collected for analysis. Prepared samples were extracted with chloroform/methanol (2: 1, v/v). The solution was centrifuged at 5000 × *g* for 5 min and the lower organic phase was used for LC- MS/MS analysis using a Orbitrap Velos Pro system (ThermoFisher), in similar with protocols used in the untargeted metabolite profiling. An aliquot of 1 μL analytes or standards was injected, and the flow rate was set at 0.3 mL/min. Standard curves were plotted and the level of 24-HC in relative to the amounts of samples was calculated.

Oscillibacter isolation and grafting

Gut contents from capsaicin-treated 5xFAD mice were collected under anaerobic conditions (5% H_2, 20% CO_2, 75% N_2). Bacterial strains were

isolated by serial streaking and plating on YCFA agar supplemented with 0.1% taurocholate, followed by incubation at 37 °C for up to 1 week. Purified *Oscillibacter* isolates were identified via whole-genome sequencing on Illumina NovaSeq 6000 platform, assembled with SPAdes, and annotation with Prokka. Species-level assignment was confirmed using fastANI for average nucleotide identity with ANI ≥ 98% against reference metagenomic species in accordance with previous studies[17]. Isolates were cultured in YCFAC broth at 37 °C under anaerobic conditions, and sealed for preservation at −80 °C in PBS with 40% glycerol and 0.001% L-cysteine. Frozen samples were thawed at 4 °C for 12 h prior to use and subsequently administered to 5-month 5xFAD mice via oral gavage.

Cell culturing and treatment

Murine BV2 cell (RRID: CVCL_0182, obtained from Mingjin Biotech, Shanghai, China) was maintained in high-glucose DMEM–pyruvate medium (11995065, Gibco) supplemented with 10% fetal bovine serum (10099141, Gibco) and 1% penicillin–streptomycin (15140122, Gibco). Before Aβ and 24-HC treatment, BV2 cells were serum-starved for 12 h, and then activated by incubation with 100 ng/mL LPS for 12 h. 10 μM Aβ1-42 oligomers in combination with DMSO or increasing doses of 24-HC (0.01, 0.1, 1, 10 μM) were incubated for 4.5 or 24 h before harvest. For LXRβ knock-down, transient transfection of plasmids was performed using a Lipofectamine 3000 transfection reagent (Invitrogen). The sequences of siRNA were 5′ -ACGCUUACACCUCAGCCUA-3′ (sense) and 5′ -UAGGCUGAGGUGUGUAAGCGU-3′ (antisense). siRNAs, plasmids and virus were constructed by OBIO (Shanghai, China).

For primary culturing of mouse microglia, cortices and hippocampi of newborn (P0) C57BL/6 mouse pups were collected, enzymatically dissociated with trypsin, and followed by trypsin inhibitor and DNase I treatment. Dissociated cells were plated onto PDL-coated T-75 flasks in DMEM supplemented with 10% FBS and maintained at 37 °C, 5% CO_2. After 5 days when astrocytes formed a confluent layer, microglia growing atop were isolated by vigorously tapping the flasks, floating cells enriched for microglia were collected, counted, coated onto DMEM, and then maintained at 37 °C, 5% CO_2. In similar with BV2 cells, microglia were activated by LPS, and then incubated with 10 μM $A\beta_{42}$ oligomers +10 μM 24-HC for 4.5 or 24 h before harvest.

MTT assay

BV2 cells were incubated with vehicle (DMSO) and increasing doses of 24-HC (0.01 μM ~ 10 mM) for 24 h. Then, 1.1 mM MTT (3-(4,5-dimethylthiazol-2-yl)−2,5-diphenyltetrazolium bromide) was added into the medium and incubated at 37 °C (5% CO_2) for 2 h. After removal of MTT, DMSO was added to dissolve formazan crystals. Absorbance at 570 nm was measured using a Varioskan LUX Multimode Microplate Reader (Thermo Fisher). Cell viability (%) was calculated by normalizing the absorbance of Veh- or 24-HC-treated samples to untreated controls × 100.

Flow cytometry

BV2 Cells were harvested following drug treatment, dead cells were stained with Fixable Viability Dye eFluor™ 660 (65-0864-14, eBioscience) and exclude from analysis. Live BV2 cells were fixed with 4% paraformaldehyde, diluted and washed using a flow cytometry staining buffer (00-4222-26, eBioscience), then stained with PE-conjugated CD206, FITC-conjugated CD86, and PE-Cyanine7-conjugated CD16/32 antibodies, and identified using a cytometer (LSRFortessa, BD, USA). Fluorescein-conjugated IgG2a kappa isotype controls (eBioscience) were used for background staining. Data were analyzed using FlowJo v10.0 (BD, USA). A figure exemplifying the gating strategy for flow cytometry is provided in the Supplementary Fig. S13.

Brain stereotaxic injection

Mice weighting 20 – 35 g were anesthetized with isoflurane, and fixed in a stereotaxic instrument (RWD, China). The scalp was sterilized with 75% ethanol and incised along the skull midline. Holes were drilled at posterior 1.9 mm and lateral ±1.1 mm from the bregma, and AAVs were injected into the dorsal CA1 at ventral −1.5 from the skull using an automatic microinjection system (World Precision Instruments, USA) at the rate of 0.05 μL/min. The needle syringe was left in place for 5 min before withdrawal. The skin was sutured and sterilized with iodophors.

Golgi staining and neurites analysis

Mice were deeply anesthetized and perfused with PBS for 5 min, and brains were removed. Golgi staining were performed as we have previously described[110], using a Rapid GolgiStain Kit (PK401, FD neurotechnologies, USA) according to the manufacturer's instructions. Images were taken using a Nikon microscope was used to image the dendrites and spine morphology, and Image-Pro Plus 6.0 was used to analyze the data. For statistical analyses, an average of 5–7 neurons per mouse (with 3 mice per group) were used and the number of spines per 10 lm of a dendrite per neuron was counted. Images were taken by a digital slide scanner (Pannoramic SCAN II, 3DHISTECH) or under the 100× oil lens of microscopy (DMI 4000B, Leica). Only pyramid neurons in hippocampal CA1 were selected for analysis. The length and spin number of secondary-branching apical dendrites were measured.

Electron microscopy

Mice hippocampal tissues were isolated, fixed in 2.5% glutaraldehyde at 4 °C for 24 h, washed in 0.1 M PBS, and post-fixed in 1% osmium acid for 2 h. After washed with PBS, samples were dehydrated in increasing gradient of ethanol, and incubated in turn with acetone/epoxy (2:1), acetone/epoxy (1:1) and epoxy, respectively, each for 12 h at 37 °C. Subsequently, obtained specimens were embedded in epoxy at 37 °C for 48 h, and sections of 100 nm thickness were sliced using a ultramicrotome (EM UC7, Leica), stained in a buffer containing 2% uranium acetate and lead citrate at room temperature for 15 min. Images were taken by a transmission electron microscope (JEM-1400, JEOL), and analyzed using Fiji.

CLEIA

A volume of 600 μL plasma sample from each participant was vortexed, and then centrifuged at 2000 × *g* for 5 min, the supernatant was collected and subsequently transferred to specific cuvettes. The concentration of p-tau217, p-tau181, NfL, Aβ1-42 and Aβ1-40 was measured, respectively, using a fully-automated LUMIPULSE G1200 Analyzer (Fujirebio Europe, Ghent, Belgium) and commercial kit for the detection of each biomarker (Supplementary Data 7). All procedures followed the manufacturer's instructions.

Statistics & reproducibility

This study employed a single-blind design for data collection and statistical analysis. Group allocation for animals or other biological samples was performed in a pseudo-randomized manner. The number of biological replicates was determined based on standard practice, typically ensuring a sample size of N ≥ 3 per group, with N ≥ 7 in mouse behavioral experiments. All experimental findings were independently replicated by different researchers to ensure reproducibility. No data were excluded from the analyses. Statistical analyses were performed using SPSS Statistics (v24.0.0, IBM), R (v2022.12.0) or GraphPad Prism (v10.1.2, GraphPad Software). Statistical methods used for analysis were as illustrated in each figure legend. $P \le 0.05$ was considered as statistically significant. Figures were plotted using GraphPad Prism, R, unless otherwise specified. Certain illustrative components within the figures were created in BioRender. Zheng, J. (2026) https://BioRender.com/c9dsmfb, and are utilized in compliance with their licensing terms (agreement number AR298KV6BT).

Reporting summary

Further information on research design is available in the Nature Portfolio Reporting Summary linked to this article.

Data availability

Source Data are provided with this paper as a Source Data file. Bulk RNA and metagenome sequencing data generated in this study have been deposited in the NCBI-SRA database under accession code PRJNA1173896, PRJNA1173905, respectively. Metabolome data generated in this study are provided in the Supplementary Data 5. Source data are provided with this paper.

References

1. Long, J. M. & Holtzman, D. M. Alzheimer disease: An update on pathobiology and treatment strategies. *Cell* **179**, 312–339 (2019).
2. Mei, C. et al. Advances of therapy for Alzheimer's disease: An updated review. *Brain-X* **2**, e68 (2024).
3. Hershey, M. S. et al. Prevention of Alzheimer's disease and cognitive decline with diet and lifestyle: Proceedings of the A. G. Leventis Foundation Conference. *J. Prev. Alzheimers Dis.* **10**, 137–143 (2023).
4. Barnes, L. L. et al. Trial of the MIND diet for prevention of cognitive decline in older persons. *N. Engl. J. Med.* **389**, 602–611 (2023).
5. Inyang, D., Saumtally, T., Nnadi, C. N., Devi, S. & So, P. W. a systematic review of the effects of capsaicin on Alzheimer's disease. *Int. J. Mol. Sci.* **24**, 10176 (2023).
6. Gimenez, B. L., Nascimento, D. O. A. T., Vassiliades, S. V. & Parise-Filho, R. Natural and synthetic capsaicin analogues: A comprehensive review of biological effects and synthetic pathways. *Curr. Med. Chem*. 10-2174 (2024).
7. Zhu, G., Zhao, J., Zhang, H., Wang, G. & Chen, W. Gut microbiota and its metabolites: Bridge of dietary nutrients and Alzheimer's disease. *Adv. Nutr.* **14**, 819–839 (2023).
8. Liang, Y. et al. The link between gut microbiome and Alzheimer's disease: From the perspective of new revised criteria for diagnosis and staging of Alzheimer's disease. *Alzheimers Dement.* **20**, 5771–5788 (2024).
9. Ferreiro, A. L. et al. Gut microbiome composition may be an indicator of preclinical Alzheimer's disease. *Sci. Transl. Med.* **15**, eabo2984 (2023).
10. Xia, Y. et al. Bacteroides Fragilis in the gut microbiomes of Alzheimer's disease activates microglia and triggers pathogenesis in neuronal C/EBPβ transgenic mice. *Nat. Commun.* **14**, 5471 (2023).
11. Grabrucker, S. et al. Microbiota from Alzheimer's patients induce deficits in cognition and hippocampal neurogenesis. *Brain* **146**, 4916–4934 (2023).
12. Chen, C. et al. Gut microbiota regulate Alzheimer's disease pathologies and cognitive disorders via PUFA-associated neuroinflammation. *Gut* **11**, 2233–2252 (2022).
13. Kim, N. et al. Transplantation of gut microbiota derived from Alzheimer's disease mouse model impairs memory function and neurogenesis in C57BL/6 mice. *Brain. Behav. Immun.* **98**, 357–365 (2021).
14. Zhang, Y. et al. Transmission of Alzheimer's disease-associated microbiota dysbiosis and its impact on cognitive function: Evidence from mice and patients. *Mol. Psychiatry* **28**, 4421–4437 (2023).
15. Kim, M. S. et al. Transfer of a healthy microbiota reduces amyloid and tau pathology in an Alzheimer's disease animal model. *Gut* **69**, 283–294 (2020).
16. Wang, F. et al. Extraction, purification, bioactivity and pharmacological effects of capsaicin: a review. *Crit. Rev. Food Sci. Nutr.* **62**, 5322–5348 (2022).
17. Li, C. et al. Gut microbiome and metabolome profiling in Framingham heart study reveals cholesterol-metabolizing bacteria. *Cell* **187**, 1834–1852 (2024).
18. Le, H. H., Lee, M. T., Besler, K. R., Comrie, J. & Johnson, E. L. Characterization of interactions of dietary cholesterol with the murine and human gut microbiome. *Nat. Microbiol.* **7**, 1390–1403 (2022).
19. Yao, L. et al. A biosynthetic pathway for the selective sulfonation of steroidal metabolites by human gut bacteria. *Nat. Microbiol.* **7**, 1404–1418 (2022).
20. Kenny, D. J. et al. Cholesterol metabolism by uncultured human gut bacteria influences host cholesterol level. *Cell Host Microbe* **28**, 245–257 (2020).
21. Ahmed, H. et al. Brain cholesterol and Alzheimer's disease: Challenges and opportunities in probe and drug development. *Brain* **147**, 1622–1635 (2024).
22. van der Kant, R. et al. Cholesterol metabolism is a druggable axis that independently regulates tau and amyloid-beta in iPSC-derived Alzheimer's disease neurons. *Cell Stem Cell* **24**, 363–375 (2019).
23. Oakley, H. et al. Intraneuronal beta-amyloid aggregates, neurodegeneration, and neuron loss in transgenic mice with five familial Alzheimer's disease mutations: potential factors in amyloid plaque formation. *J. Neurosci.* **26**, 10129–10140 (2006).
24. Forner, S. et al. Systematic phenotyping and characterization of the 5xFAD mouse model of Alzheimer's disease. *Sci. Data.* **8**, 270 (2021).
25. AmeliMojarad, M. & AmeliMojarad, M. The neuroinflammatory role of microglia in Alzheimer's disease and their associated therapeutic targets. *CNS Neurosci. Ther.* **30**, e14856 (2024).
26. Woodburn, S. C., Bollinger, J. L. & Wohleb, E. S. The semantics of microglia activation: neuroinflammation, homeostasis, and stress. *J. Neuroinflamm.* **18**, 258 (2021).
27. Da, S. A. et al. Lipopolysaccharide-induced animal models for neuroinflammation - An overview. *J. Neuroimmunol.* **387**, 578273 (2024).
28. Story, G. M. et al. ANKTM1, a TRP-like channel expressed in nociceptive neurons, is activated by cold temperatures. *Cell* **112**, 819–829 (2003).
29. Caterina, M. J., Rosen, T. A., Tominaga, M., Brake, A. J. & Julius, D. A capsaicin-receptor homologue with a high threshold for noxious heat. *Nature* **398**, 436–441 (1999).
30. Oz, M., Lorke, D. E. & Howarth, F. C. Transient receptor potential vanilloid 1 (TRPV1)-independent actions of capsaicin on cellular excitability and ion transport. *Med. Res. Rev.* **43**, 1038–1067 (2023).
31. Loh, J. S. et al. Microbiota-gut-brain axis and its therapeutic applications in neurodegenerative diseases. *Signal Transduct. Target. Ther.* **9**, 37 (2024).
32. Schaible, P., Henschel, J. & Erny, D. How the gut microbiota impacts neurodegenerative diseases by modulating CNS immune cells. *J. Neuroinflamm.* **22**, 60 (2025).
33. Latorre-Leal, M. et al. CYP46A1-mediated cholesterol turnover induces sex-specific changes in cognition and counteracts memory loss in ovariectomized mice. *Sci. Adv.* **10**, eadj1354 (2024).
34. Mast, N., Li, Y. & Pikuleva, I. A. Increased acetylcholine levels and other brain effects in 5XFAD mice after treatment with 8,14-dihydroxy metabolite of efavirenz. *Int. J. Mol. Sci.* **23**, 7669 (2022).
35. Petrov, A. M. & Pikuleva, I. A. Cholesterol 24-hydroxylation by CYP46A1: Benefits of modulation for brain diseases. *Neurotherapeutics* **16**, 635–648 (2019).
36. Dai, D. et al. GMrepo v2: A curated human gut microbiome database with special focus on disease markers and cross-dataset comparison. *Nucleic Acids Res.* **50**, D777–D784 (2022).

37. Troci, A. et al. Disease- and stage-specific alterations of the oral and fecal microbiota in Alzheimer's disease. *PNAS Nexus* **3**, pgad427 (2023).
38. Cirstea, M. S. et al. The oral and fecal microbiota in a Canadian cohort of Alzheimer's disease. *J. Alzheimers Dis.* **87**, 247–258 (2022).
39. Vogt, N. M. et al. Gut microbiome alterations in Alzheimer's disease. *Sci. Rep.* **7**, 13537 (2017).
40. Mahalak, K. K. et al. Analysis of the ability of capsaicin to modulate the human gut microbiota in vitro. *Nutrients* **14**, 1283 (2022).
41. Kwon, H. S. & Koh, S. H. Neuroinflammation in neurodegenerative disorders: The roles of microglia and astrocytes. *Transl. Neurodegener.* **9**, 42 (2020).
42. Nishi, T. et al. Soticlestat, a novel cholesterol 24-hydroxylase inhibitor shows a therapeutic potential for neural hyperexcitation in mice. *Sci. Rep.* **10**, 17081 (2020).
43. Courtney, R. & Landreth, G. E. LXR regulation of brain cholesterol: From development to disease. *Trends Endocrinol. Metab.* **27**, 404–414 (2016).
44. Zhang, Y., Luo, X. Y., Wu, D. H. & Xu, Y. ROR nuclear receptors: Structures, related diseases, and drug discovery. *Acta Pharmacol. Sin.* **36**, 71–87 (2015).
45. Im, S. S. & Osborne, T. F. Liver x receptors in atherosclerosis and inflammation. *Circ. Res.* **108**, 996–1001 (2011).
46. Ghisletti, S. et al. Parallel SUMOylation-dependent pathways mediate gene- and signal-specific transrepression by LXRs and PPAR. *Mol. Cell.* **25**, 57–70 (2007).
47. Lin, R. et al. Directed evolution of adeno-associated virus for efficient gene delivery to microglia. *Nat. Methods* **19**, 976–985 (2022).
48. Chen, Y. & Yu, Y. Tau and neuroinflammation in Alzheimer's disease: interplay mechanisms and clinical translation. *J. Neuroinflamm.* **20**, 165 (2023).
49. van der Kant, R., Goldstein, L. & Ossenkoppele, R. Amyloid-beta-independent regulators of tau pathology in Alzheimer disease. *Nat. Rev. Neurosci.* **21**, 21–35 (2020).
50. Yoshiyama, Y. et al. Synapse loss and microglial activation precede tangles in a P301S tauopathy mouse model. *Neuron* **53**, 337–351 (2007).
51. Ising, C. et al. NLRP3 inflammasome activation drives tau pathology. *Nature* **575**, 669–673 (2019).
52. Nishizono, I. et al. Rapid and sensitive chemiluminescent enzyme immunoassay for measuring tumor markers. *Clin. Chem.* **37**, 1639–1644 (1991).
53. Liu, C. H. et al. The associations between a capsaicin-rich diet and blood amyloid-beta levels and cognitive function. *J. Alzheimers Dis.* **52**, 1081–1088 (2016).
54. Wang, J. et al. Capsaicin consumption reduces brain amyloid-beta generation and attenuates Alzheimer's disease-type pathology and cognitive deficits in APP/PS1 mice. *Transl. Psychiatry* **10**, 230 (2020).
55. Shi, Z. et al. High chili intake and cognitive function among 4582 adults: An open cohort study over 15 years. *Nutrients* **11**, 1183 (2019).
56. Corral-Guerrero, I. A. et al. Capsaicin as a microbiome modulator: Metabolic interactions and implications for host health. *Metabolites* **15**, 372 (2025).
57. Xiang, Q. et al. Capsaicin, the spicy ingredient of chili peppers: Effects on gastrointestinal tract and composition of gut microbiota at various dosages. *Foods* **11**, 686 (2022).
58. Gong, T. et al. Capsaicin regulates lipid metabolism through modulation of bile acid/gut microbiota metabolism in high-fat-fed SD rats. *Food Nutr. Res.* **66**, https://doi.org/10.29219/fnr.v66.8289 (2022).
59. Rollyson, W. D. et al. Bioavailability of capsaicin and its implications for drug delivery. *J. Control. Release* **196**, 96–105 (2014).
60. Reilly, C. A., Crouch, D. J., Yost, G. S. & Fatah, A. A. Determination of capsaicin, nonivamide, and dihydrocapsaicin in blood and tissue by liquid chromatography-tandem mass spectrometry. *J. Anal. Toxicol.* **26**, 313–319 (2002).
61. Fernandes, E. S., Fernandes, M. A. & Keeble, J. E. The functions of TRPA1 and TRPV1: moving away from sensory nerves. *Br. J. Pharmacol.* **166**, 510–521 (2012).
62. Kang, C. et al. Gut microbiota mediates the protective effects of dietary capsaicin against chronic low-grade inflammation and associated obesity induced by high-fat diet. *Mbio* **8**, e00417–e00470 (2017).
63. Song, J. X. et al. Dietary capsaicin improves glucose homeostasis and alters the gut microbiota in obese diabetic ob/ob mice. *Front. Physiol.* **8**, 602 (2017).
64. Baboota, R. K. et al. Capsaicin-induced transcriptional changes in hypothalamus and alterations in gut microbial count in high fat diet fed mice. *J. Nutr. Biochem.* **25**, 893–902 (2014).
65. Shen, W. et al. Anti-obesity effect of capsaicin in mice fed with high-fat diet is associated with an increase in population of the gut bacterium Akkermansia muciniphila. *Front. Microbiol.* **8**, 272 (2017).
66. Liu, P. et al. Altered microbiomes distinguish Alzheimer's disease from amnestic mild cognitive impairment and health in a Chinese cohort. *Brain. Behav. Immun.* **80**, 633–643 (2019).
67. Ueda, A. et al. Identification of Faecalibacterium prausnitzii strains for gut microbiome-based intervention in Alzheimer's-type dementia. *Cell Rep. Med.* **2**, 100398 (2021).
68. Yang, X., Yu, D., Xue, L., Li, H. & Du, J. Probiotics modulate the microbiota-gut-brain axis and improve memory deficits in aged SAMP8 mice. *Acta Pharm. Sin. B.* **10**, 475–487 (2020).
69. Bjorkhem, I. & Meaney, S. Brain cholesterol: Long secret life behind a barrier. *Arterioscler. Thromb. Vasc. Biol.* **24**, 806–815 (2004).
70. Lutjohann, D. et al. Cholesterol homeostasis in human brain: Evidence for an age-dependent flux of 24S-hydroxycholesterol from the brain into the circulation. *Proc. Natl. Acad. Sci. USA* **93**, 9799–9804 (1996).
71. Jiang, Z. et al. Lipid-lowering efficacy of the capsaicin in patients with metabolic syndrome: A systematic review and meta-analysis of randomized controlled trials. *Front. Nutr.* **9**, 812294 (2022).
72. Wang, Y., Tang, C., Tang, Y., Yin, H. & Liu, X. Capsaicin has an anti-obesity effect through alterations in gut microbiota populations and short-chain fatty acid concentrations. *Food Nutr. Res.* **64**, https://doi.org/10.29219/fnr.v64.3525 (2020).
73. Xiang, Q. et al. Capsaicin—the spicy ingredient of chili peppers: A review of the gastrointestinal effects and mechanisms. *Trends Food Sci. Technol.* **116**, 755–765 (2021).
74. Petrov, A. M. et al. CYP46A1 activation by efavirenz leads to behavioral improvement without significant changes in amyloid plaque load in the brain of 5XFAD mice. *Neurotherapeutics* **16**, 710–724 (2019).
75. Testa, G. et al. A silver lining for 24-hydroxycholesterol in Alzheimer's disease: The involvement of the neuroprotective enzyme sirtuin 1. *Redox Biol.* **17**, 423–431 (2018).
76. Gamba, P. et al. The controversial role of 24-s-hydroxycholesterol in Alzheimer's disease. *Antioxidants*. **10**, 740 (2021).
77. Gc, J. B. et al. Molecular basis for the recognition of 24-(S)-hydroxycholesterol by integrin αvβ3. *Sci. Rep.* **13**, 9166 (2023).
78. Choi, H. et al. 25-Hydroxycholesterol modulates microglial function and exacerbates Alzheimer's disease pathology: Mechanistic insights and therapeutic potential of cholesterol esterification inhibition. *J. Neuroinflamm.* **22**, 50 (2025).
79. Romero, J., Toral-Rios, D., Yu, J., Paul, S. M. & Cashikar, A. G. 25-hydroxycholesterol promotes brain cytokine production and

leukocyte infiltration in a mouse model of lipopolysaccharide-induced neuroinflammation. *J. Neuroinflamm.* **21**, 251 (2024).
80. Wong, M. Y. et al. 25-Hydroxycholesterol amplifies microglial IL-1β production in an apoE isoform-dependent manner. *J. Neuroinflamm.* **17**, 192 (2020).
81. Sodero, A. O. 24S-hydroxycholesterol: Cellular effects and variations in brain diseases. *J. Neurochem.* **157**, 899–918 (2021).
82. Tsitsou-Kampeli, A. et al. Cholesterol 24-hydroxylase at the choroid plexus contributes to brain immune homeostasis. *Cell Rep. Med.* **4,** 101278 (2023).
83. Mast, N. et al. Cholesterol-metabolizing enzyme cytochrome P450 46A1 as a pharmacologic target for Alzheimer's disease. *Neuropharmacology* **123**, 465–476 (2017).
84. Zelcer, N. et al. Attenuation of neuroinflammation and Alzheimer's disease pathology by liver x receptors. *Proc. Natl. Acad. Sci. USA* **104**, 10601–10606 (2007).
85. Lee, J. H. et al. Differential SUMOylation of LXRalpha and LXRbeta mediates transrepression of STAT1 inflammatory signaling in IFN-gamma-stimulated brain astrocytes. *Mol. Cell.* **35**, 806–817 (2009).
86. Ghisletti, S. et al. Parallel SUMOylation-dependent pathways mediate gene- and signal-specific transrepression by LXRs and PPARgamma. *Mol. Cell.* **25**, 57–70 (2007).
87. Leng, F. & Edison, P. Neuroinflammation and microglial activation in Alzheimer disease: where do we go from here? *Nat. Rev. Neurol.* **17**, 157–172 (2021).
88. Seo, D. et al. ApoE isoform- and microbiota-dependent progression of neurodegeneration in a mouse model of tauopathy. *Sci. (N. Y., N. Y.).* **379**, eadd1236 (2023).
89. Wei, X., Nishi, T., Kondou, S., Kimura, H. & Mody, I. Preferential enhancement of GluN2B-containing native NMDA receptors by the endogenous modulator 24S-hydroxycholesterol in hippocampal neurons. *Neuropharmacology* **148**, 11–20 (2019).
90. Paul, S. M. et al. The major brain cholesterol metabolite 24(S)-hydroxycholesterol is a potent allosteric modulator of N-methyl-D-aspartate receptors. *J. Neurosci.* **33**, 17290–17300 (2013).
91. Testa, G. et al. 24-hydroxycholesterol induces tau proteasome-dependent degradation via the SIRT1/PGC1alpha/Nrf2 pathway: A potential mechanism to counteract Alzheimer's disease. *Antioxidants*. **12**, (2023).
92. Abildayeva, K. et al. 24(S)-hydroxycholesterol participates in a liver X receptor-controlled pathway in astrocytes that regulates apolipoprotein E-mediated cholesterol efflux. *J. Biol. Chem.* **281**, 12799–12808 (2006).
93. Gamba, P. et al. Interaction between 24-hydroxycholesterol, oxidative stress, and amyloid-beta in amplifying neuronal damage in Alzheimer's disease: three partners in crime. *Aging Cell* **10**, 403–417 (2011).
94. Ferguson, E. L. et al. Independent associations of high-density lipoprotein cholesterol and triglyceride levels with Alzheimer's disease and related dementias. *Alzheimers Dement.* **21**, e14575 (2025).
95. Luo, J. et al. Genetic associations between modifiable risk factors and Alzheimer disease. *JAMA Netw. Open.* **6**, e2313734 (2023).
96. Reed, B. et al. Associations between serum cholesterol levels and cerebral amyloidosis. *JAMA Neurol.* **71**, 195–200 (2014).
97. Tcw, J. et al. Cholesterol and matrisome pathways dysregulated in astrocytes and microglia. *Cell* **185**, 2213–2233 (2022).
98. Ding, J. et al. APOE4 Exacerbates Cerebral Tau Pathology Through Cholesterol-Induced Degradation of Phosphatase in Atherosclerosis. *CNS Neurosci. Ther.* **31**, e70536 (2025).
99. Ren, Z. et al. Increased intestinal bile acid absorption contributes to age-related cognitive impairment. *Cell Rep. Med.* 101543 (2024).
100. Chen, T. et al. Metabolic phenotyping reveals an emerging role of ammonia abnormality in Alzheimer's disease. *Nat. Commun.* **15**, 3796 (2024).
101. Wang, B. & Tontonoz, P. Liver X receptors in lipid signalling and membrane homeostasis. *Nat. Rev. Endocrinol.* **14**, 452–463 (2018).
102. Jack, C. J. et al. NIA-AA Research Framework: Toward a biological definition of Alzheimer's disease. *Alzheimers Dement.* **14**, 535–562 (2018).
103. Sasmita, A. O. et al. Parental origin of transgene modulates amyloid-beta plaque burden in the 5xFAD mouse model of Alzheimer's disease. *Neuron* **113**, 838–846 (2025).
104. Xiao, Y. et al. A tau dephosphorylation-targeting chimera selectively recruits protein phosphatase-1 to ameliorate Alzheimer's disease and tauopathies. *Cell Chem. Biol.* **31**, 1787–1799 (2024).
105. Schindelin, J. et al. Fiji: An open-source platform for biological-image analysis. *Nat. Methods* **9**, 676–682 (2012).
106. Bolger, A. M., Lohse, M. & Usadel, B. Trimmomatic: A flexible trimmer for Illumina sequence data. *Bioinformatics* **30**, 2114–2120 (2014).
107. Langmead, B. & Salzberg, S. L. Fast gapped-read alignment with Bowtie 2. *Nat. Methods* **9**, 357–359 (2012).
108. Li, D., Liu, C. M., Luo, R., Sadakane, K. & Lam, T. W. MEGAHIT: An ultra-fast single-node solution for large and complex metagenomics assembly via succinct de Bruijn graph. *Bioinformatics* **31**, 1674–1676 (2015).
109. Gurevich, A., Saveliev, V., Vyahhi, N. & Tesler, G. QUAST: Quality assessment tool for genome assemblies. *Bioinformatics* **29**, 1072–1075 (2013).
110. Su, J. et al. Generation of tau dephosphorylation-targeting chimeras for the treatment of Alzheimer's disease and related tauopathies. *Sci. Bull.* **69**, 1137–1152 (2024).

Acknowledgements

This work was supported in part by the Brain Science and Brain-like Intelligence Technology-National Science and Technology (2025ZD0217600, to J.Z.), the Guizhou Provincial Science and Technology Program (Qiankehe-jichu-ZK[2021]-yiban362, to Y.L.), the National Natural Science Foundation of China (82160558, to Y.L.), the Science and Technology Program of Zunyi City (Zunshikehe-HZ(2020)−252, to Y.L.), the Excellent Youth Talent Training Program of Affiliated Hospital of Zunyi Medical University (to Y.L.); the Peking University Talent Startup Fund supported by the Fundamental Research Funds for the Central Universities (BMU2022YJ003, to J.Z.), Clinical Medicine Plus X - Young Scholars Project of Peking University, the Fundamental Research Funds for the Central Universities (PKU2025PKULCXQ016, to J.Z.); the Scientific Project of Beijing Life Science Academy (2024300CC0020, to J.Z.; 2023000CA0060, to Y.W.; 2023000CB0010, to J.M.), the Supporting Project for Principle Investigators of Beijing Life Science Academy (2024302RPIB03, to Y.W.); and the Opening Project of Hubei Key Laboratory of Cognitive and Affective Disorders (HBCAD2024-03, to J.Z.).

Author contributions

Conceptualization: Y.L., J.Z.; Methodology: Y.L., H.W., D.Z., S.W., Y.Y., J.D., Z.W., J.Z.; Investigation: Y.L., D.Z., H.W., S.W., Z.L., J.L., S.Y., W.S., B.Y., S.T., D.T., B.W., D.L., C.B., Q.W., Y.G., H.Y., J.Z.; Data analysis: Y.L., D.Z., S.W., K.C., C.L., Y.Y., J.Z.; Manuscript writing: Y.L., D.Z., J.Z.; Manuscript revision: Y.L., J.M., F.L., Y.W., J.Y., X.L., J.Z.; Funding acquisition: Y.L., J.Y., J.M., Y.W., J.Z.; Resources: Y.L., J.Y., X.L., J.Z.; Supervision: Y.L., F.L., Y.W., J.Y., X.L., J.Z.

Competing interests

The authors declare no competing interests.

Additional information

Supplementary information The online version contains supplementary material available at https://doi.org/10.1038/s41467-026-68937-9.

Correspondence and requests for materials should be addressed to Junliang Yuan, Xuemei Liu or Jie Zheng.

Peer review information *Nature Communications* thanks Mauro Costa-Mattioli, Silvia Maioli, Inhee Mook-Jung, and the other, anonymous, reviewer for their contribution to the peer review of this work. A peer review file is available.

[1]Department of Gastroenterology, Affiliated Hospital of Zunyi Medical University, Zunyi, China. [2]Digestive Disease Hospital, Affiliated Hospital of Zunyi Medical University, Zunyi, China. [3]Neuroscience Research Institute, Peking University, Beijing, China. [4]Department of Neurobiology, School of Basic Medical Sciences, Peking University, Beijing, China. [5]Key Laboratory for Neuroscience, Ministry of Education/National Health Commission, Peking University, Beijing, China. [6]Beijing Life Science Academy, Beijing, China. [7]Key Laboratory of Basic Pharmacology of Ministry of Education, Zunyi Medical University, Zunyi, Guizhou, China. [8]Joint International Research Laboratory of Ethnomedicine of Ministry of Education, Zunyi Medical University, Zunyi, Guizhou, China. [9]Chinese Phramcological Society-Guizhou Province Joint Laboratory for Pharmacology, Zunyi Medical University, Zunyi, Guizhou, China. [10]Department of Neurology, Peking University Sixth Hospital, Peking University Institute of Mental Health, NHC Key Laboratory of Mental Health (Peking University), National Clinical Research Center for Mental Disorders (Peking University Sixth Hospital), Beijing 100191, China. [11]Key Laboratory of Human Brain bank for Functions and Diseases of Department of Education of Guizhou Province, Guizhou Medical University, Guiyang, China. [12]Key Laboratory of Endemic and Ethnic Diseases of Ministry of Education, School of Forensic Medicine, Guizhou Medical University, Guiyang, China. [13]Department of Neurology, Renmin Hospital of Wuhan University, Wuhan, China. [14]Center for Neurodegenerative Disease Research, Renmin Hospital of Wuhan University, Wuhan, China. [15]Department of Radiology, Zhongnan Hospital of Wuhan University, Wuhan University, Wuhan, China. [16]Department of Fundamental Medicine, Wuxi School of Medicine, Jiangnan University, Wuxi, China. [17]These authors contributed equally: Yawen Li, Hui Wang, Dongyuan Zhang, Shiqi Wang. ✉e-mail: junliangyuan@bjmu.edu.cn; onlyoneliuxuemei@163.com; zhengjiie@hsc.pku.edu.cn